

## Role of Higgs and Leggett modes for the third harmonic response in noncentrosymmetric superconductors

S. Klein\* and D. Manske

*Max Planck Institute for Solid State Research, 70569 Stuttgart, Germany*

(Received 25 March 2024; revised 18 June 2024; accepted 21 June 2024; published 12 July 2024)

The amplitude and phase of the third harmonic response in superconductors provide important insights into collective Higgs and Leggett modes, respectively, in the superconducting state. In particular, for twice the incident frequency equal to the binding energy ( $2\omega = 2\Delta$ ), one finds a resonance of the amplitude and a corresponding phase jump in the third harmonic response, respectively. We generalize these concepts to superconductors without an inversion symmetry, which can be effectively described by a two-band model with an order parameter consisting of spin-singlet (even parity) and spin-triplet (odd parity) components. In our work we use an effective action approach for the derivation of the nonlinear response and assign the underlying physical processes to their respective Feynman diagrams. We calculate the third harmonic signal exemplary for the noncentrosymmetric compound CePt<sub>3</sub>Si, showing that it contains contributions from three distinguishable sources, namely the Higgs mode, the Leggett mode, and quasiparticles (broken Cooper-pairs). Only in the clean limit diamagnetic Raman-like processes contribute to the third harmonic signal, whereas the quasiparticle contributions dominate the collective modes for all triplet-singlet ratios of the gap structure. In the dirty limit, we find a significant enhancement of the Higgs mode contributions to the third harmonic response, due to the inclusion of nonvanishing paramagnetic diagrams. Finally, we argue that the phase difference between the third harmonic and the fundamental signal might reveal a jump, where its size is dependent on the light-matter coupling.

DOI: [10.1103/PhysRevB.110.014510](https://doi.org/10.1103/PhysRevB.110.014510)

### I. INTRODUCTION

In the past few years, Higgs spectroscopy has emerged as a powerful tool to investigate the properties of superconductors, with experiments able to excite the amplitude (Higgs) mode of the  $U(1)$ -broken phase. In clean superconductors, Higgs modes are coupled only nonlinearly to light and are therefore visible in nonlinear optical spectroscopic techniques, such as Raman and third-harmonic response, often called third harmonic generation (THG) [1–9]. A resonance in the THG intensity appears, when matching the driving frequency to the energy of the Higgs mode  $2\omega = 2\Delta$ . At that resonance frequency a phase jump occurs in the phase difference between third harmonic and fundamental signal. On the other hand, dirty superconductors reveal an enhanced signal that can be detected with linear coupling to light [10,11].

It has been demonstrated that the THG and other superconducting response differs according to the symmetry of the gap function, which can be used for a classification of the Higgs mode [12]. This response was already discussed

in detail for gap symmetries with even parity, such as  $s$ - or  $d$ -wave superconductors, where the THG and phase jump was calculated [1,7,13]. However, recently, also gap functions with odd parity were analyzed in more detail [14].

In noncentrosymmetric superconductors (NCSs), the Rashba-type antisymmetric spin-orbit coupling (ASOC) is caused by the absence of an inversion center and leads to a lifting of the band degeneracy. Thus, a single-band superconductor might be effectively described in a two-band structure. Additionally, this absence leads to a breakdown of the strict separation between even-parity spin-singlet and odd-parity spin-triplet pairing correlations, thus allows for a mixed-symmetry pairing interaction forming Cooper pairs [15–18]. This results in a mixed parity order parameter, formed by a superposition of spin-singlet and spin-triplet components, affecting the response of collective modes [19]. The prototypical noncentrosymmetric tetragonal superconductor CePt<sub>3</sub>Si is only one example of such materials without an inversion symmetry and was already the target of various extensive theoretical [17,20–28] and experimental studies [29–37].

So far the investigation of superconductive collective modes has involved systems with spin-singlet (mainly  $s$ - and  $d$ -wave) pairing states, either single- or multiband. In the former case, only the amplitude mode has been investigated, since, at least in 2D superconductors, the Goldstone mode does not directly contribute to the electromagnetic response at zero external momentum hence to the THG. The reason for that is the gauge invariance, that allows the phase mode to be gauged away by its coupling to the density mode [38]. In

\*Contact author: [s.klein@fkf.mpg.de](mailto:s.klein@fkf.mpg.de)

the latter, additionally to the amplitude modes of each band, a Leggett phase mode appears mostly inside the superconducting gap. This Leggett mode describes the Josephson-like oscillations between the phases of the two superconducting order parameters and corresponds therefore to collective fluctuations of the superconducting interband phase difference.

Noncentrosymmetric superconductors can be effectively described as two-band superconductors, each of them has a restored inversion symmetry. Therefore, analogously to singlet multiband superconductors, both Higgs and Leggett modes are present in the superconducting response [19]. However, neither a signature of the response of collective modes in NCSs has not been calculated so far, nor the nonlinear THG process. Only the influence of quasiparticles in parity-violated NCSs in the Raman signal [39] as well as the second harmonic generation (SHG) [40] have been studied recently. These uncovered points of interest will be addressed in this paper, where we get a deeper understanding of the THG signal contributions in NCSs caused by quasiparticles, the Higgs mode and the Leggett mode, respectively, by analyzing both intensity and phase signals. In fact, it has been recently shown in conventional and unconventional superconductors that the phase of the generated harmonics contains additional information about the collective modes and impurity level of the superconductor [41]. Furthermore, our discussion will go beyond the clean limit and cover also the paramagnetic response by including an extended Mattis-Bardeen approximation. In centrosymmetric superconductors it has been shown that the influence of impurities lead to a strong enhancement of the THG signal, especially for the Higgs response [42–44]. As we assumed a similar behavior for NCS, we aim for a generalization of the resulting THG signal for the Higgs mode in the dirty limit.

The paper is organized as follows: in Sec. II we develop the theoretical background, introducing the minimal model Hamiltonian with ASOC which allows to describe a crystal structure without inversion symmetry. Thus, we carry out the basis transformation which allows a two-band symmetric picture. In Sec. III we use an effective-action approach to derive the amplitude and phase fluctuations. For a better understanding of the underlying physical processes we also illustrate the accordant relevant Feynman diagrams. Afterwards, we calculate and analyze the generation of third-harmonic by the superconductor in intensity and phase, as a function of frequency and temperature. This is done in the clean limit (Sec. IV) as well as in the influence of impurities (Sec. V). Finally, in Sec. VI we compare our results with previous works on Higgs modes in superconductors before we summarize our paper in Sec. VII.

## II. FUNDAMENTALS FOR NONCENTROSYMMETRIC SUPERCONDUCTORS

We first consider the noninteracting single-particle Hamiltonian in a crystal without inversion center

$$\hat{H}_0 = \sum_{\mathbf{k}} \sum_{\sigma, \sigma'=\uparrow, \downarrow} [\epsilon_{\mathbf{k}} \delta_{\sigma\sigma'} + \mathbf{g}_{\mathbf{k}} \cdot \boldsymbol{\sigma}_{\sigma\sigma'}] \hat{a}_{\mathbf{k}\sigma}^\dagger \hat{a}_{\mathbf{k}\sigma'}, \quad (1)$$

where  $\epsilon_{\mathbf{k}}$  is the noninteracting electronic band dispersion,  $\sigma$  and  $\sigma'$  label the spin,  $\boldsymbol{\sigma}$  is the vector of the Pauli matrices and

$\hat{a}_{\mathbf{k}\sigma}^{(\dagger)}$  the annihilation (creation) operator of an electron with momentum  $\mathbf{k}$  and spin  $\sigma$ . The second term in the Hamiltonian describes the antisymmetric spin-orbit coupling (ASOC)  $\mathbf{g}_{\mathbf{k}} = (g_{\mathbf{k},x}, g_{\mathbf{k},y}, g_{\mathbf{k},z}) = -\mathbf{g}_{-\mathbf{k}}$ , whose exact form depends on the corresponding point group of the crystal. In this paper, the tetragonal point group  $\mathcal{G} = C_{4v}$  is investigated, which is the generating point group in CePt<sub>3</sub>Si (and also in CeRhSi<sub>3</sub> or CeIrSi<sub>3</sub>). The corresponding ASOC reads

$$\mathbf{g}_{\mathbf{k}} = \alpha(\hat{\mathbf{k}} \times \hat{\mathbf{e}}_z) + \alpha' \hat{k}_x \hat{k}_y \hat{k}_z (\hat{k}_x^2 - \hat{k}_y^2) \hat{\mathbf{e}}_z. \quad (2)$$

In the following, we are setting the coupling strength of the second term  $\alpha' = 0$ , so that we recover the two-dimensional Rashba interaction  $\mathbf{g}_{\mathbf{k}} = \alpha(\hat{\mathbf{k}} \times \hat{\mathbf{e}}_z)$  with ASOC strength  $\alpha$  [45].

Due to the antisymmetric spin-orbit coupling, the Kramer spin degeneracy is lifted and two bands with different spin structure are created. Accordingly, we can transform the Hamiltonian from the spin representation in the diagonal band representation by a unitary transformation [18,25,26]

$$\hat{a}_{\mathbf{k},\sigma} = \sum_{\mu=\pm 1} u_{\sigma,\mu}(\mathbf{k}) \hat{c}_{\mathbf{k},\mu}, \quad (3)$$

with

$$u_{\uparrow,\mu}(\mathbf{k}) = \sqrt{\frac{\mathbf{g}_{\mathbf{k}} + \mu \mathbf{g}_{\mathbf{k},z}}{2\mathbf{g}_{\mathbf{k}}}}, \quad (4a)$$

$$u_{\downarrow,\mu}(\mathbf{k}) = \mu \frac{g_{\mathbf{k},x} + i g_{\mathbf{k},y}}{\sqrt{2\mathbf{g}_{\mathbf{k}}(\mathbf{g}_{\mathbf{k}} + \mu \mathbf{g}_{\mathbf{k},z})}}, \quad (4b)$$

and  $\mathbf{g}_{\mathbf{k}} = |\mathbf{g}_{\mathbf{k}}|$ . Then the Hamiltonian becomes

$$\hat{H}_0 = \sum_{\mathbf{k}} \sum_{\mu=\pm 1} \xi_{\mathbf{k},\mu} \hat{c}_{\mathbf{k},\mu}^\dagger \hat{c}_{\mathbf{k},\mu}, \quad (5)$$

where its eigenvalues

$$\xi_{\mathbf{k},\mu} = \epsilon_{\mathbf{k}} + \mu \mathbf{g}_{\mathbf{k}} \quad (6)$$

corresponds to two distinct energy bands ( $\mu = \pm 1$ ).

We now consider the presence of a superconducting instability generated by a weak electron-electron interaction of the Bardeen-Cooper-Schrieffer form in the original spin basis. Thus, the interacting Hamiltonian reads

$$\hat{H}_{\text{int}} = -\frac{1}{2} \sum_{\mathbf{k}, \mathbf{k}'} \sum_{\substack{\alpha, \beta, \\ \gamma, \delta=\uparrow, \downarrow}} V_{\mathbf{k}, \mathbf{k}'}^{\alpha\beta\gamma\delta} \hat{a}_{\mathbf{k},\alpha}^\dagger \hat{a}_{-\mathbf{k},\beta}^\dagger \hat{a}_{-\mathbf{k}',\gamma} \hat{a}_{\mathbf{k}',\delta}. \quad (7)$$

In particular, we use a general ansatz for the pairing interaction introduced in Refs. [15,17,18],

$$\begin{aligned} V_{\mathbf{k}, \mathbf{k}'}^{\alpha\beta\gamma\delta} &= W^g (i\sigma_2)_{\alpha,\beta} (i\sigma_2)_{\gamma,\delta}^\dagger \\ &+ W^u g_{\mathbf{k},n} (i\sigma_n \sigma_y)_{\alpha\beta} g_{\mathbf{k}',l} (i\sigma_l \sigma_y)_{\gamma\delta}^\dagger \\ &+ W^m (i\sigma_2)_{\alpha,\beta} g_{\mathbf{k}',l} (i\sigma_l \sigma_y)_{\gamma\delta}^\dagger \\ &+ W^m g_{\mathbf{k},n} (i\sigma_n \sigma_y)_{\alpha\beta} (i\sigma_2)_{\gamma,\delta}^\dagger, \end{aligned} \quad (8)$$

with the pairing constants  $W^g$ ,  $W^u$ , and  $W^m$ , describing the conventional even ( $g$ ) parity pairing and the triplet odd ( $u$ ) parity pairing, as well as a scattering of Cooper pairs between the two channels ( $m$ ). Here, we used the Pauli matrices  $\sigma_{l,n=x,y,z}$  which act in the fermionic spin basis.

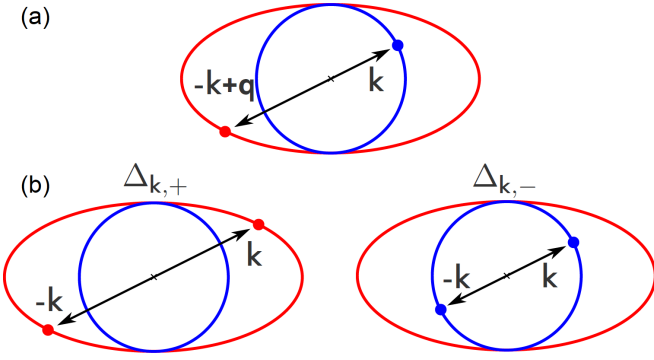


FIG. 1. Schematics of the polar plot of the gap functions showing the neglected (a) and favored (b) Cooper pairings. The two bands ( $\mu = +$  in red and  $\mu = -$  in blue) are splitted due to the antisymmetric spin-orbit coupling strength  $\alpha$ . This ASOC strength is much larger than the order parameter  $\Delta$ . This requires a finite momentum  $\mathbf{q}$  (for almost all directions) for the pair function, leading to a suppressed interband interaction in panel (a). Only intraband interactions in panel (b) are contributing to the system.

Using the unitary transformation with components of Eq. (4), we can rewrite Eq. (7) in the band basis as follows:

$$\hat{H}_{\text{int}} = - \sum_{\mathbf{k}, \mathbf{k}'} \sum_{\mu, \nu = \pm 1} V_{\mu, \nu; \mathbf{k}, \mathbf{k}'} \hat{c}_{\mathbf{k}, \mu}^\dagger \hat{c}_{-\mathbf{k}, \mu}^\dagger \hat{c}_{-\mathbf{k}', \nu} \hat{c}_{\mathbf{k}', \nu}, \quad (9)$$

with the pairing interaction

$$V_{\mu, \nu; \mathbf{k}, \mathbf{k}'} = W^g(\tau_0 + \tau_x)_{\mu, \nu} + W^u g_{\mathbf{k}} g_{\mathbf{k}'} (\tau_0 - \tau_x)_{\mu, \nu} - W^m [g_{\mathbf{k}}(\tau_z - i\tau_y)_{\mu, \nu} - g_{\mathbf{k}'}(\tau_z + i\tau_y)_{\mu, \nu}]. \quad (10)$$

Here, we used the Pauli matrices  $\tau_{x,y,z}$  and the identity  $\tau_0 = \mathbf{I}_{2 \times 2}$  acting in the band basis. Note that by performing the transformation, we allowed only intraband pairing. The interband pairing is usually suppressed, since the band splitting requires electrons, located far from the Fermi surfaces, to pair. For NCS typical high values of the asymmetric spin-orbit coupling compared to the superconducting energy scale ( $\alpha \gg \Delta$ ), such processes, which lead to a center of mass of the Cooper pairs, are unlikely to happen as shown in Refs. [18,20] (see also Fig. 1).

Within the BCS mean-field approximation, we can define the superconducting gap as the order parameter

$$\Delta_{\mathbf{k}, \mu} = \sum_{\mathbf{k}'} \sum_{\nu = \pm 1} V_{\mu, \nu; \mathbf{k}, \mathbf{k}'} \langle \hat{c}_{-\mathbf{k}', \nu} \hat{c}_{\mathbf{k}', \nu} \rangle, \quad (11)$$

whose corresponding self-consistent equation reads

$$\Delta_{\mathbf{k}, \mu} = \sum_{\mathbf{k}'} \sum_{\nu = \pm 1} V_{\mu, \nu; \mathbf{k}, \mathbf{k}'} \frac{\Delta_{\mathbf{k}', \nu}}{2E_{\mathbf{k}', \nu}} \tanh(\beta E_{\mathbf{k}', \nu}/2), \quad (12)$$

with the Bogoliubov quasiparticle energy for each band ( $\nu = \pm 1$ ) given by  $E_{\mathbf{k}', \nu}^2 = \xi_{\mathbf{k}', \nu}^2 + |\Delta_{\mathbf{k}', \nu}|^2$ . The gap can be expressed as a combination of spin-singlet pairing gap  $\psi_{\mathbf{k}}$  and a spin-triplet pairing gap  $\mathbf{d}_{\mathbf{k}}$ , due to the presence of ASOC [20], obtaining

$$\Delta_{\mathbf{k}, \mu} = \psi_{\mathbf{k}} + \mu |\mathbf{d}_{\mathbf{k}}|. \quad (13)$$

In particular, we consider an  $s$ -wave symmetry for the spin-singlet gap,  $\psi_{\mathbf{k}} = \psi \equiv \Delta_{\psi}$ . Moreover, it has been

demonstrated in Ref. [21] that in the limit of strong ASOC only the component  $\mathbf{d}_{\mathbf{k}} \parallel \mathbf{g}_{\mathbf{k}}$  survives for the spin-triplet gap, so that  $|\mathbf{d}_{\mathbf{k}}| = d g_{\mathbf{k}}$ .

We can also write the gap function in the factorized form  $\Delta_{\mathbf{k}, \mu} = f_{\mathbf{k}}^{\mu} \Delta_{\mu}$ , introducing appropriate mixed form factors  $f_{\mathbf{k}}^{\mu}$  and their corresponding  $\Delta_{\mu}$ . The form factor for the  $\mu = +$  band is given by

$$f_{\mathbf{k}}^+ = \frac{\psi + d g_{\mathbf{k}}}{\psi + d} \in \left[ \frac{\psi}{\psi + d}, 1 \right], \quad \Delta_{\mu=+1} = \psi + d. \quad (14)$$

For the  $\mu = -$  band the form factor can be written as

$$f_{\mathbf{k}}^- = \frac{\psi - d g_{\mathbf{k}}}{\psi} \in \left[ \frac{\psi - d}{\psi}, 1 \right], \quad \Delta_{\mu=-1} = \psi, \quad (15)$$

if  $d < 2\psi$  and

$$f_{\mathbf{k}}^- = \frac{\psi - d g_{\mathbf{k}}}{d - \psi} \in \left[ -1, \frac{\psi}{d - \psi} \right], \quad \Delta_{\mu=-1} = d - \psi, \quad (16)$$

if  $d \geq 2\psi$ , respectively.

It is instructive to plot the total resulting order parameter for various triplet-singlet ratios  $p = d/\Delta_s$  in Fig. 2. Note, that when the triplet contribution exceeds the singlet contribution, we will find nodes in specific directions in the  $\mathbf{k}$ -space. We will see later that these nodes are changing the THG signal in a characteristic way. Additionally it is worth to mention, that with increasing triplet-singlet ratio  $p$ , a faster change in the absolute value of the order parameter can be detected, especially around the  $k_z$  axis. This effect can be used later to explain increasing broadening phenomena in the spectra.

Finally, the influence of the Coulomb interaction is taken into account via the additional term in the Hamiltonian

$$H_c = \frac{1}{2} \sum_{\mathbf{k}, \mathbf{k}', \mathbf{q}} \sum_{\substack{\alpha, \beta, \\ \gamma, \delta = \uparrow, \downarrow}} V_c'(\mathbf{q}) a_{\mathbf{k}+\mathbf{q}, \alpha}^\dagger a_{\mathbf{k}, \beta} a_{\mathbf{k}'-\mathbf{q}, \gamma}^\dagger a_{\mathbf{k}', \delta}, \quad (17)$$

with the Coulomb potential  $V_c'(\mathbf{q})$ . In the band basis this Coulomb Hamiltonian transforms to

$$H_c = \frac{1}{2} \sum_{\mathbf{k}, \mathbf{k}', \mathbf{q}} \sum_{\mu \nu} V_c(\mathbf{q}) c_{\mathbf{k}+\mathbf{q}, \mu}^\dagger c_{\mathbf{k}, \mu} c_{\mathbf{k}'-\mathbf{q}, \nu}^\dagger c_{\mathbf{k}', \nu}. \quad (18)$$

For each band  $\mu = \pm 1$  we can define the corresponding Nambu-Gor'kov spinor  $\Psi_{\mathbf{k}, \mu}^\dagger = (\hat{c}_{\mathbf{k}, \mu}^\dagger \hat{c}_{-\mathbf{k}, \mu})$ , so that the interacting Hamiltonian in Eq. (9) can be rewritten as

$$\hat{H}_{\text{int}} = - \frac{1}{4} \sum_{\mathbf{k}, \mathbf{k}'} \sum_{\mu, \nu = \pm 1} V_{\mu, \nu; \mathbf{k}, \mathbf{k}'} \Psi_{\mathbf{k}, \mu}^\dagger (\tau_1 + i\tau_2) \Psi_{\mathbf{k}, \mu} \times \Psi_{\mathbf{k}', \nu}^\dagger (\tau_1 - i\tau_2) \Psi_{\mathbf{k}', \nu}, \quad (19)$$

where  $\tau_{1,2}$  are the Pauli matrices in the space of Nambu spinors. Analogously, the single-particle Hamiltonian in Eq. (5) becomes

$$\hat{H}_0 = \frac{1}{2} \sum_{\mathbf{k}} \sum_{\mu = \pm 1} \xi_{\mathbf{k}, \mu} \Psi_{\mathbf{k}, \mu}^\dagger \tau_3 \Psi_{\mathbf{k}, \mu}. \quad (20)$$

In this formalism, we can derive our two-fermions interaction terms and subsequently the Nambu Green's function  $G_{\mathbf{k}\mathbf{k}', \mu}$  of the system. This derivation is presented in the Appendix and

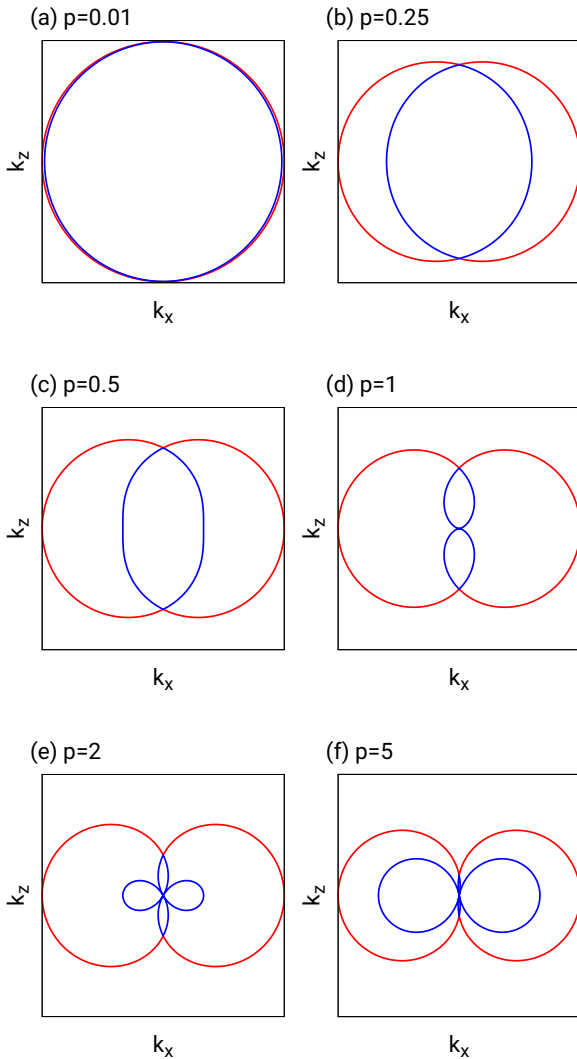


FIG. 2. Symmetry of the order parameters. The plots show the 2D- $k_x k_z$  symmetry structure of the order parameters  $|\Delta_{\mathbf{k},\mu}|$  of the two bands ( $\mu = +1$  in red,  $\mu = -1$  in blue) of CePt<sub>3</sub>Si for different triplet-singlet ratios  $p = d/\Delta_s$  at  $k_y = 0$ . (a) For low  $p$  ( $p = 0.01$ ) the singlet  $s$ -wave gap symmetry dominates and therefore the two gaps are nearly degenerate and rotationally invariant. (b), (c) Increasing  $p$ , and therefore the contribution of the triplet component, the degeneracy of the gaps is lifted and they possess only  $C_2$  rotational symmetry. (d) For  $p = 1$ , the singlet and triplet gap contribute equally, leading to a vanishing gap in the  $\mu = -1$  band for  $k_z = 0$ . (e), (f) If the triplet component is larger than the singlet (i.e.,  $p > 1$ ), then one obtains additional nodes for the  $\mu = -$  band.

will be used in the following section to calculate the THG response in NCS.

### III. THEORY FOR THIRD HARMONIC RESPONSE IN NONCENTROSYMMETRIC SUPERCONDUCTORS

In the following, two approaches to calculate the THG signal in NCS are instructively discussed. We start with the derivation of the effective action via a Hubbard-Stratonovich transformation in Sec. III A. Afterwards, we write down and calculate the corresponding Feynman diagrams in Sec. III B,

where we also consider Coulomb screening in the system. Finally, we illustrate the changes in the calculation, when going from a clean to a dirty superconductor via a Mattis-Bardeen approximation in Sec. III C.

#### A. Effective action approach

The dynamics of the model transformed Hamiltonian  $H = H_0 + H_{\text{int}}$  in Eqs. (19)–(20) can be introduced in a path-integral formulation with the imaginary-time action

$$S(\Psi, \Psi^\dagger) = \int_0^{1/T} d\tau \left( \sum_{\mathbf{k}, \mu} \Psi_{\mathbf{k}, \mu}^\dagger \partial_\tau \Psi_{\mathbf{k}, \mu} + H \right). \quad (21)$$

The partition function is then given by the functional integral

$$Z = \int D(\Psi, \Psi^\dagger) e^{-S(\Psi, \Psi^\dagger)}. \quad (22)$$

In the following, we will take advantage of a separable pairing interaction  $V_{\mu, \nu; \mathbf{k}, \mathbf{k}'} = V_{\mu\nu} f_{\mathbf{k}}^\mu f_{\mathbf{k}'}^\nu$ , so that the  $\mathbf{k}$ -dependence of the effective action is significantly simplified. As a next step, the interacting term in the exponent of the partition function  $Z$  can be decoupled by a Hubbard-Stratonovich transformation to investigate the physics of the collective fluctuations around the mean-field solution

$$S(\Psi, \Psi^\dagger) = \int_0^{1/T} d\tau \left( \sum_{\mu\nu} V_{\mu\nu}^{-1} \Delta_{\mu}^* \Delta_{\nu}^{\prime} - \sum_{\mathbf{k}\mathbf{k}', \mu} \Psi_{\mathbf{k}, \mu}^\dagger G_{\mathbf{k}\mathbf{k}', \mu}^{-1} \Psi_{\mathbf{k}', \mu} \right). \quad (23)$$

Here, the bosonic complex fields  $\Delta_{\pm}^{\prime}$  and  $\Delta_{\pm}^{\prime}$ , representing the fluctuations of the superconducting order parameter in amplitude and phase, were introduced. An additional gauge field  $\mathbf{A}$  representing the coupling to light is implemented via Peierls substitution  $c_{\mu}^{\dagger} c_{\mu} \rightarrow c_{\mu}^{\dagger} c_{\mu} e^{i\mathbf{A}}$  which modifies only the kinetic part of the Hamiltonian.

Consequently, the fluctuations around the mean-field value of the superconducting fields  $\Delta_{\mu, \text{eq}}$  are decomposed in amplitude  $\Delta_{\mu}(\tau)$  and phase  $\theta_{\mu}(\tau)$  fluctuations

$$\Delta_{\mu}^{\prime}(\tau) \rightarrow \Delta_{\mu, \text{eq}} + \Delta_{\mu}(\tau) + i\theta_{\mu}(\tau). \quad (24)$$

Note that without loss of generality, we have assumed a real equilibrium gap, i.e.,  $\text{Im}(\Delta_{\mu, \text{eq}}) = 0$ . This allows us to treat the amplitude fluctuations as oscillations along the real axis (in  $\tau_1$  channel) and the phase fluctuations as oscillations parallel to the imaginary axis (in  $\tau_2$  channel) of the order parameter  $\Delta$ . After integrating over the fermions the action reads then

$$S(\Psi, \Psi^\dagger) = \int_0^{1/T} d\tau \sum_{\mu\nu} V_{\mu\nu}^{-1} [\Delta_{\mu, \text{eq}}^* \Delta_{\nu, \text{eq}} + \Delta_{\mu}^*(\tau) \Delta_{\nu}(\tau) + \theta_{\mu}^*(\tau) \theta_{\nu}(\tau)] - \sum_{\mu} \text{Tr} \ln (-G_{\mu}^{-1}), \quad (25)$$

where the trace includes the summation over momentum and frequency. Expanding the effective action in powers of the

bosonic fields around their mean-field value leads to

$$\text{Tr} \ln (-G_\mu^{-1}) = \text{Tr} \ln (-G_0^{-1}) - \sum_{n \geq 1} \frac{\text{Tr}(G_0 \Sigma)^n}{n}, \quad (26)$$

with the self-energy for the fluctuating fields  $\Sigma$ . This allows us to split the action  $S = S_{\text{MF}} + S_{\text{FL}}$  in a time-independent mean-field part

$$S_{\text{MF}} = \sum_{\mu\nu} \frac{\Delta_{\mu,\text{eq}}^* \Delta_{\nu,\text{eq}}}{TV_{\mu\nu}} - \text{Tr} \ln (-G_0^{-1}), \quad (27)$$

and a fluctuating quartic-order part

$$S_{\text{FL}}^{(4)} = \frac{T}{2} \sum_{i\omega_m} \left[ \sum_{ijkl,\mu} A_{ij}^2(-i\omega_m) \chi_{A^2 A^2}^{ijkl,\mu}(i\omega_m) A_{kl}^2(i\omega_m) + \phi^T(-i\omega_m) b(i\omega_m) + b^T(-i\omega_m) \phi(i\omega_m) + \phi^T(-i\omega_m) \overleftrightarrow{M}(i\omega_m) \phi(i\omega_m) \right]. \quad (28)$$

$$\overleftrightarrow{M}(i\omega_m) = \begin{pmatrix} \frac{2V_{--}}{V} + \chi_{\Delta,\Delta}^+(i\omega_m) & \frac{-2V_{+-}}{V} & -\chi_{\Delta,\lambda}^+(i\omega_m) & 0 \\ \frac{-2V_{+-}}{V} & \frac{2V_{++}}{V} + \chi_{\Delta,\Delta}^-(i\omega_m) & 0 & -\chi_{\Delta,\lambda}^-(i\omega_m) \\ -\chi_{\lambda,\Delta}^+(i\omega_m) & 0 & \frac{2V_{--}}{V} + \chi_{\lambda\lambda}^+(i\omega_m) & \frac{-2V_{+-}}{V} \\ 0 & -\chi_{\lambda,\Delta}^-(i\omega_m) & \frac{-2V_{+-}}{V} & \frac{2V_{++}}{V} + \chi_{\lambda\lambda}^-(i\omega_m) \end{pmatrix}, \quad (31)$$

with  $V = \det V_{\mu\nu}$ . In Eqs. (28), (30), and (31) we introduced the susceptibilities  $\chi_{\alpha,\beta}^i$ . Their indices  $\alpha$  and  $\beta$  represent thereby the coupling between light  $A$ , the Higgs mode  $\Delta$  and the Leggett mode  $\lambda$ , occurring via the phase fluctuations  $\theta$ . In Sec. III B, we will assign these susceptibilities to Feynman diagrams and present their derivation in Eqs. (39)–(41) and Eqs. (45)–(46).

Finally, after integrating out the fluctuations, the quartic order action in Eq. (28) reads

$$S_{\text{FL}}^{(4)} = \frac{T}{2} \sum_{i\omega_m} \left[ \sum_{ijkl,\mu} A_{ij}^2(-i\omega_m) \chi_{A^2 A^2}^{ijkl,\mu}(i\omega_m) A_{kl}^2(i\omega_m) + b^T(-i\omega_m) \overleftrightarrow{M}^{-1}(i\omega_m) b(i\omega_m) \right], \quad (32)$$

and the third harmonic current is given after analytic continuation by

$$j^{(3)}(3\Omega) = - \left. \frac{\delta S_{\text{FL}}^{(4)}}{\delta A(-\omega)} \right|_{3\Omega}. \quad (33)$$

To get a more realistic solution of the THG response calculations also Coulomb screening has to be taken into account. This can be modeled by including an additional Coulomb term to the Hamiltonian

$$H_c = \frac{1}{2} \sum_{\mathbf{k}, \mathbf{k}', \mathbf{q}} \sum_{\mu\nu} V_c(\mathbf{q}) c_{\mathbf{k}+\mathbf{q},\mu}^\dagger c_{\mathbf{k},\mu} c_{\mathbf{k}'-\mathbf{q},\nu}^\dagger c_{\mathbf{k}',\nu}, \quad (34)$$

The vector containing the fluctuating fields reads

$$\phi^T(i\omega_m) = (\Delta_+(i\omega_m), \Delta_-(i\omega_m), \theta_+(i\omega_m), \theta_-(i\omega_m)), \quad (29)$$

where their fluctuations are described by the coupling to light

$$b(i\omega_m) = \begin{pmatrix} -\sum_{ij} A_{ij}^2(i\omega_m) \chi_{\Delta,A^2}^{ij,+}(i\omega_m) \\ -\sum_{ij} A_{ij}^2(i\omega_m) \chi_{\Delta,A^2}^{ij,-}(i\omega_m) \\ \sum_{ij} A_{ij}^2(i\omega_m) \chi_{\lambda,A^2}^{ij,+}(i\omega_m) \\ \sum_{ij} A_{ij}^2(i\omega_m) \chi_{\lambda,A^2}^{ij,-}(i\omega_m) \end{pmatrix} \quad (30)$$

and their interaction with themselves, visible in the matrix

with Coulomb potential  $V_c(\mathbf{q})$ . For the effective action a density field  $\rho'(\tau) = \rho_{\text{eq}} + \rho(\tau)$  is introduced, which couples to the other fields in the fluctuating action part which leads to the extended mean-field action

$$S_{\text{MF}} = \sum_{\mu\nu} \frac{\Delta_{\mu,\text{eq}}^* \Delta_{\nu,\text{eq}}}{TV_{\mu\nu}} - \frac{\rho_{\text{eq}}^* \rho_{\text{eq}}}{TV_c(\mathbf{q})} - \text{Tr} \ln (-G_0^{-1}), \quad (35)$$

and the following five-component vectors for the fluctuating part  $S_{\text{FL}}^C$  in Eq. (28)

$$\phi^T(i\omega_m) = (\Delta_+(i\omega_m), \Delta_-(i\omega_m), \theta_+(i\omega_m), \theta_-(i\omega_m), \rho(i\omega_m)), \quad (36)$$

$$b(i\omega_m) = \begin{pmatrix} -\sum_{ij} A_{ij}^2(i\omega_m) \chi_{\Delta,A^2}^{ij,+}(i\omega_m) \\ -\sum_{ij} A_{ij}^2(i\omega_m) \chi_{\Delta,A^2}^{ij,-}(i\omega_m) \\ \sum_{ij} A_{ij}^2(i\omega_m) \chi_{\lambda,A^2}^{ij,+}(i\omega_m) \\ \sum_{ij} A_{ij}^2(i\omega_m) \chi_{\lambda,A^2}^{ij,-}(i\omega_m) \\ -\sum_{ij,\mu} A_{ij}^2(i\omega_m) \chi_{A^2,\rho}^{ij,\mu}(i\omega_m) \end{pmatrix}. \quad (37)$$



The corresponding  $5 \times 5$  matrix reads then

$$\vec{M}(i\omega_m) = \begin{pmatrix} \frac{2V_{-+}}{V} + \chi_{\Delta,\Delta}^+(i\omega_m) & \frac{-2V_{+-}}{V} & -\chi_{\Delta,\lambda}^-(i\omega_m) & 0 & \chi_{\Delta,\rho}^+(i\omega_m) \\ \frac{-2V_{+-}}{V} & \frac{2V_{++}}{V} + \chi_{\Delta,\Delta}^-(i\omega_m) & 0 & -\chi_{\Delta,\lambda}^-(i\omega_m) & \chi_{\Delta,\rho}^-(i\omega_m) \\ -\chi_{\lambda,\Delta}^-(i\omega_m) & 0 & \frac{2V_{-+}}{V} + \chi_{\lambda\lambda}^+(i\omega_m) & \frac{-2V_{+-}}{V} & -\chi_{\lambda,\rho}^+(i\omega_m) \\ 0 & -\chi_{\lambda,\Delta}^-(i\omega_m) & \frac{-2V_{+-}}{V} & \frac{2V_{++}}{V} + \chi_{\lambda\lambda}^-(i\omega_m) & -\chi_{\lambda,\rho}^-(i\omega_m) \\ \chi_{\Delta,\rho}^+(i\omega_m) & \chi_{\Delta,\rho}^-(i\omega_m) & -\chi_{\lambda,\rho}^+(i\omega_m) & -\chi_{\lambda,\rho}^-(i\omega_m) & -\frac{1}{v_c(\mathbf{q})} + \sum_{\mu} \chi_{\lambda,\rho}^{\mu}(i\omega_m) \end{pmatrix}. \quad (38)$$

Note, that the coupling terms  $\chi_{\Delta,\lambda}^+(i\omega_m)$  and  $\chi_{\Delta,\lambda}^-(i\omega_m)$  are odd in  $\xi_{\mathbf{k}}$  and therefore rely on an asymmetric distribution of states close to the Fermi surface. This means that in general this coupling is strongly suppressed and can be neglected in the following. Similar arguments can be found for the coupling terms  $\chi_{\lambda,\rho}^+(i\omega_m)$  and  $\chi_{\lambda,\rho}^-(i\omega_m)$ .

### B. Diagrammatic approach

From our effective action approach, we can extract contributions from the quasiparticles, as well as collective mode contributions in the amplitude (Higgs) and phase (Leggett) channel. The arising contributions are also shown as Feynman diagrams in Table I. In the amplitude channel we find contributions of two distinguishable Higgs modes  $H_{\mu\nu}$  on their corresponding bands ( $\mu = \nu$ ), which are coupled with band-mixing contributions. In the phase channel, the relative phase/Leggett mode  $L_{\mu\nu}$  ( $\mu \neq \nu$ ) contributions are dominant in the analyzed frequency range, while the sum phase/Goldstone mode is neglectable. The shown diagrams consist of the corresponding propagators for each mode as well as their connecting bubbles. In the clean limit diagrams with two-photon vertices  $\gamma_{ij} = \partial^2 \xi_{\mathbf{k}} / \partial k_i \partial k_j$  are the most dominant contributions and their single bubble susceptibility are given by

$$\chi_{\Delta A^2}^{ij,\nu}(i\omega_m) = \sum_{\mathbf{k}} f_{\mathbf{k}} \frac{1}{2} \gamma_{ij}^2 X_{13}^{\nu}(\mathbf{k}, i\omega_m), \quad (39)$$

$$\chi_{\lambda A^2}^{ij,\nu}(i\omega_m) = \sum_{\mathbf{k}} f_{\mathbf{k}} \frac{1}{2} \gamma_{ij}^2 X_{23}^{\nu}(\mathbf{k}, i\omega_m), \quad (40)$$

$$\chi_{A^2 A^2}^{ijkl,\nu}(i\omega_m) = \sum_{\mathbf{k}} \frac{1}{4} \gamma_{ij}^2 \gamma_{kl}^2 X_{33}^{\nu}(\mathbf{k}, i\omega_m), \quad (41)$$

with

$$X_{\alpha\beta}^{\nu}(\mathbf{k}, i\omega_m) = T \sum_{i\omega_n} \text{tr} [G_0^{\nu}(\mathbf{k}, i\omega_n) \tau_{\alpha} G_0^{\nu}(\mathbf{k}, i\omega_n + i\omega_m) \tau_{\beta}], \quad (42)$$

and the Nambu Green's function  $G_0$  given in the Appendix.

Note that the Green's function inside one bubble are considered on the same band, as the contributions from interband bubbles has been proven to be neglectable small in the system. The indices of the susceptibilities are showing their integration to the diagrams via vertices to photons (A), the amplitude propagator ( $H$ ), and the phase propagator ( $\lambda$ ), respectively.

The propagators of their corresponding collective modes are given in the form of RPA series (see Fig. 3) for the Higgs

mode

$$H(i\omega_m)_{\mu\nu} = V_{\mu\nu} + \sum_{\theta} V_{\mu\theta} \chi_{\Delta\Delta}^{\theta}(i\omega_m) H(i\omega_m)_{\theta\nu}, \quad (43)$$

and the Leggett mode

$$L(i\omega_m)_{\mu\nu} = V_{\mu\nu} + \sum_{\theta} V_{\mu\theta} \chi_{\lambda\lambda}^{\theta}(i\omega_m) L(i\omega_m)_{\theta\nu}, \quad (44)$$

with the susceptibilities

$$\chi_{\Delta\Delta}^{\nu}(i\omega_m) = \sum_{\mathbf{k}} f_{\mathbf{k},\nu}^2 X_{11}^{\nu}(\mathbf{k}, i\omega_m), \quad (45)$$

$$\chi_{\lambda\lambda}^{\nu}(i\omega_m) = \sum_{\mathbf{k}} f_{\mathbf{k},\nu}^2 X_{22}^{\nu}(\mathbf{k}, i\omega_m). \quad (46)$$

With the obtained propagators we can describe the THG response of the arising contributions for the quasiparticles, the Higgs mode and the Leggett mode in the short form

$$\chi_{\text{QP}}^{\text{dia}}(i\omega_m) = \sum_{\nu} \chi_{A^2 A^2}^{\nu}(i\omega_m), \quad (47)$$

$$\chi_{\text{H}}^{\text{dia}}(i\omega_m) = \sum_{\mu\nu} \chi_{\Delta A^2}^{\mu}(i\omega_m) \chi_{\Delta A^2}^{\nu}(i\omega_m) H_{\mu\nu}(i\omega_m), \quad (48)$$

$$\chi_{\lambda}^{\text{dia}}(i\omega_m) = \sum_{\mu\nu} \chi_{\lambda A^2}^{\mu}(i\omega_m) \chi_{\lambda A^2}^{\nu}(i\omega_m) L_{\mu\nu}(i\omega_m). \quad (49)$$

Finally, we have to include the Coulomb screening in our system. The Coulomb interaction renormalizes the

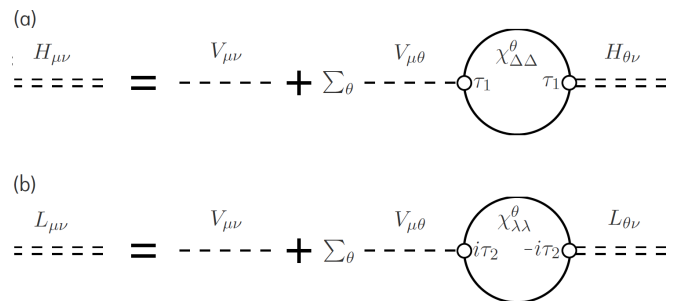
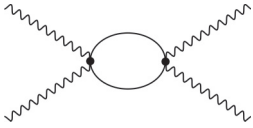
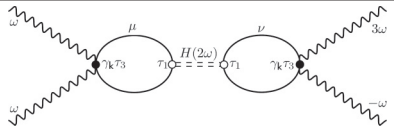
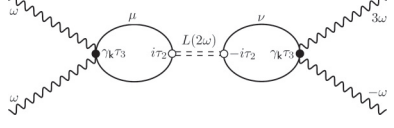
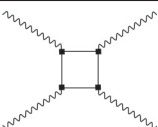
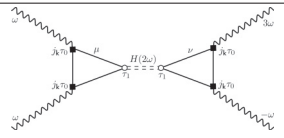
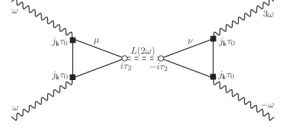


FIG. 3. Feynman diagrams of the RPA summation of collective modes. (a) The Higgs propagator  $H_{\mu\nu}$  in Eq. (43) is calculated in a multiband ( $\theta$ ) RPA series in the amplitude channel  $\tau_1$ . (b) Analogously, the Leggett propagator  $L_{\mu\nu}$  in Eq. (44) is derived in the phase channel  $\tau_2$ . The here shown susceptibility bubbles  $\chi_{\Delta\Delta}^{\theta}$  and  $\chi_{\lambda\lambda}^{\theta}$  are derived in Eqs. (45) and (46).

TABLE I. Overview over the different diagrams contributing to the THG signal. Here we differentiate between contributions coming from quasiparticles (QP), the Higgs mode, and the Leggett mode. While only the diamagnetic diagrams (top three rows) are present in the clean limit, the paramagnetic contributions (bottom three rows) are dominating, when impurities are included in the system. In the first row, the typical  $\gamma_{\mathbf{k}}\tau_3-\gamma_{\mathbf{k}}\tau_3$  bubble of broken Cooper pairs (quasiparticle excitations) in the clean limit is visible. The properties of the two modes ( $\mu = +$  and  $\mu = -$ ) of the Higgs response ( $\tau_1$ ) as well as the single mode Leggett response ( $\tau_2$ ) are shown in row two and three, respectively. The summary of our results in the last two columns (amplitude and phase THG signal) provide information about a strong suppression of the collective modes by the quasiparticles. In the following three rows the correspondent assisted THG diagrams, connected via a  $\tau_0$ -vertex, in the paramagnetic channel give all a relatively similar contribution to the THG signal, as it is visible in the relative THG amplitude. Another major differences between the diamagnetic and paramagnetic diagrams is the change in the phase jump at the THG resonances. Here we calculate a sudden change of the phase jump from  $\pi/2$  to  $\pi$ , when going from a clean superconductor to the dirty limit.

channel	clean limit?	diagram	origin	# collective modes	relative THG amplitude $I/I_{QP}^{\text{dia}}$	phase jump
dia-mag.	✓		QP	0 (continuum)	$\approx 10^0$	$\approx \pi/2$
dia-mag.	✓		Higgs	2 ( $\mu = \nu$ )	$\approx 10^{-6}$	$\approx \pi/2$
dia-mag.	✓		Leggett	1 ( $\mu \neq \nu$ )	$\approx 10^{-4}$	$\approx \pi/2$
para-mag.	✗		QP	0 (continuum)	$\approx 10^5$	$\approx \pi$
para-mag.	✗		Higgs	2 ( $\mu = \nu$ )	$\approx 10^4$	$\approx \pi$
para-mag.	✗		Leggett	1 ( $\mu \neq \nu$ )	$\approx 10^3$	$\approx \pi$

corresponding diagrams so that the resulting susceptibilities read in the limit of  $\mathbf{q} \rightarrow 0$  and  $1/V_c(\mathbf{q}) \rightarrow 0$ ,

$$\chi_{\Delta A^2}^{C,v}(i\omega_m) = \chi_{\Delta A^2}^v(i\omega_m) - \frac{\chi_{\Delta\rho}^v(i\omega_m)\chi_{A^2\rho}^v(i\omega_m)}{\chi_{\rho\rho}^v(i\omega_m)}, \quad (50)$$

$$\chi_{A^2 A^2}^{C,v}(i\omega_m) = \chi_{A^2 A^2}^v(i\omega_m) - \frac{\chi_{A^2\rho}^v(i\omega_m)\chi_{A^2\rho}^v(i\omega_m)}{\chi_{\rho\rho}^v(i\omega_m)}, \quad (51)$$

$$\chi_{\Delta\Delta}^{C,v}(i\omega_m) = \chi_{\Delta\Delta}^v(i\omega_m) - \frac{\chi_{\Delta\rho}^v(i\omega_m)\chi_{\Delta\rho}^v(i\omega_m)}{\chi_{\rho\rho}^v(i\omega_m)}, \quad (52)$$

with

$$\chi_{\Delta\rho}^v(i\omega_m) = \sum_{\mathbf{k}} f_{\mathbf{k},v} X_{13}^v(\mathbf{k}, i\omega_m), \quad (53)$$

$$\chi_{\rho\rho}^v(i\omega_m) = \sum_{\mathbf{k}} X_{33}^v(\mathbf{k}, i\omega_m), \quad (54)$$

$$\chi_{A^2\rho}^v(i\omega_m) = \sum_{\mathbf{k}} \frac{1}{2} \gamma_{ij}^2 X_{33}^v(\mathbf{k}, i\omega_m). \quad (55)$$

A diagrammatic description of this inclusion of the Coulomb screening can be seen in the renormalized vertices in Fig. 4 which illustrates Eq. (51) exemplary.

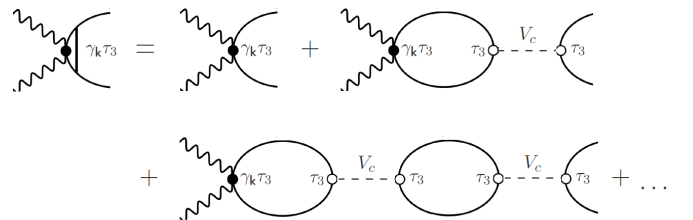


FIG. 4. Exemplary Feynman Diagram of the effective vertex renormalization for the Coulomb screening. The Coulomb interaction  $V_c$  is introduced by renormalizing in this case the vertex of incoming light  $\gamma_{\mathbf{k}}\tau_3$  into an effective vertex with the help of an RPA series.

### C. Role of impurities for THG

In the clean limit only a diamagnetic coupling of light to the condensate contributes to the collective modes as the paramagnetic response vanishes. However, it can be shown that nonmagnetic impurities are allowing an additional paramagnetic coupling [1,11]. These additional occurring diagrams are visible in the bottom half of Table I, where the light-coupling vertices are now in the  $\tau_0$  channel. Even for small disorder the paramagnetic contributions become important and are usually dominating the optical nonlinear response. To include the impurities, we will choose a Mattis-Bardeen approximation [46] to model the impurities with an effective vertex approximation.

For the implementation of the Mattis-Bardeen approximation we follow closely references [11] and [47] in which the susceptibility of the paramagnetic diagrams in Table I for the quasiparticles  $\chi_{QP}$ , Higgs  $\chi_H$  mode, and Leggett mode  $\chi_\lambda$ , respectively, are given as

$$\chi_{QP}^{\text{para}}(i\omega_m) = \sum_v \chi_{AAA}^v(i\omega_m), \quad (56)$$

$$\chi_H^{\text{para}}(i\omega_m) = \sum_{\mu\nu} \chi_{AA\Delta}^\mu(i\omega_m) \chi_{AA\Delta}^\nu(i\omega_m) H_{\mu\nu}(i\omega_m), \quad (57)$$

$$\chi_\lambda^{\text{para}}(i\omega_m) = \sum_{\mu\nu} \chi_{AA\lambda}^\mu(i\omega_m) \chi_{AA\lambda}^\nu(i\omega_m) L_{\mu\nu}(i\omega_m), \quad (58)$$

with the triangular and square bubbles defined as

$$\begin{aligned} \chi_{AA\Delta}^v(i\omega_l, i\omega_m) &= T \sum_{i\omega_n} \sum_{\mathbf{k}, \mathbf{k}'} |J_{\mathbf{k}\mathbf{k}'}^v|^2 \text{tr}[G_0^v(\mathbf{k}, i\omega_n) \tau_1 \\ &\quad \times G_0^v(\mathbf{k}, i\omega_n + i\omega_m) \\ &\quad \times G_0^v(\mathbf{k}', i\omega_n + i\omega_m + i\omega_l)], \end{aligned} \quad (59)$$

$$\begin{aligned} \chi_{AA\lambda}^v(i\omega_l, i\omega_m) &= T \sum_{i\omega_n} \sum_{\mathbf{k}, \mathbf{k}'} |J_{\mathbf{k}\mathbf{k}'}^v|^2 \text{tr}[G_0^v(\mathbf{k}, i\omega_n) \tau_2 \\ &\quad \times G_0^v(\mathbf{k}, i\omega_n + i\omega_m) \\ &\quad \times G_0^v(\mathbf{k}', i\omega_n + i\omega_m + i\omega_l)], \end{aligned} \quad (60)$$

$$\begin{aligned} \chi_{AAAA}^v(i\omega_l, i\omega_m, i\omega_p) &= T \sum_{i\omega_n} \sum_{\mathbf{k}, \mathbf{k}', \mathbf{k}''} |J_{\mathbf{k}\mathbf{k}'}^v|^2 |J_{\mathbf{k}\mathbf{k}''}^v|^2 \\ &\quad \times \text{tr}[G_0^v(\mathbf{k}, i\omega_n) G_0^v(\mathbf{k}', i\omega_n + i\omega_m) \\ &\quad \times G_0^v(\mathbf{k}, i\omega_n + i\omega_m + i\omega_l)] \\ &\quad \times G_0^v(\mathbf{k}'', i\omega_n + i\omega_m + i\omega_l + i\omega_p)]. \end{aligned} \quad (61)$$

The corresponding transition matrix element  $J_{\mathbf{k}\mathbf{k}'} = \langle \mathbf{k} | \mathbf{e} \mathbf{p} / m | \mathbf{k}' \rangle$  is approximated by a Lorentzian distribution

$$|J_{\mathbf{k}\mathbf{k}'}^v|^2 \propto \frac{W(\xi_{\mathbf{k}}^v, \xi_{\mathbf{k}'}^v)}{N(0)} = \frac{\gamma}{N(0)(\xi_{\mathbf{k}}^v - \xi_{\mathbf{k}'}^v)^2 + \gamma^2}, \quad (62)$$

with the density of states at the Fermi surface  $N(0)$  and the scattering rate  $\gamma$  revealing the strength of impurity (see Fig. 5). For  $\gamma \gg 2\Delta$  the condensate is considered in the dirty limit. Due to this photon distribution in momentum and energy, the here implemented approximation leads to an effective broadening of the Fermi surface. In Sec. V, we use

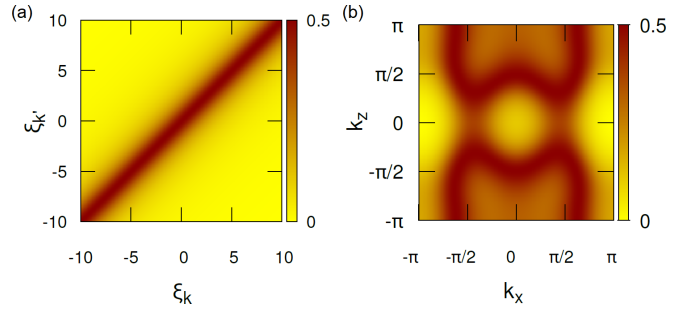


FIG. 5. Illustration of the smeared out Fermi surface in a Mattis-Bardeen-like approximation (a) The Mattis Bardeen approximation leads to a Lorentz distribution in the excitation spectra  $W(\epsilon, \epsilon')$  around the originally frequency  $\omega = \epsilon' - \epsilon = 0$  [see Eq. (62)]. The here chosen damping factor  $\gamma = 2$  represent the strength of impurities in the system. (b) By inserting this distribution into the energy dispersion in Eq. (63), one obtains a smeared out Fermi surface.

Eqs. (59), (60), and (61) to calculate the THG susceptibilities in the presence of impurities.

### IV. RESULTS IN THE CLEAN LIMIT

In this section, we will study the results of our calculated THG spectra and identify the arising modes. We will start first in the clean limit, before artificially adding impurities to our system in Sec. V.

To describe the so-called  $\beta$ -band of CePt<sub>3</sub>Si [48] without antiferromagnetic order, we will use the following expression for the tight-binding band dispersion:

$$\begin{aligned} \epsilon_{\mathbf{k}} &= 2t(\cos(k_x) + \cos(k_y)) + 4t_1 \cos(k_x) \cos(k_y) \\ &\quad + 2t_2(\cos(2k_x) + \cos(2k_y)) + 2t_3 \cos(k_z) \\ &\quad + 4t_4(\cos(k_x) + \cos(k_y)) \cos(k_z) \\ &\quad + 4t_5(\cos(2k_x) + \cos(2k_y)) \cos(k_z) \\ &\quad + 2t_6 \cos(2k_z) - \mu^*, \end{aligned} \quad (63)$$

with hopping parameters  $t, t_1/t = -0.15, t_2/t = -0.5, t_3/t = -0.3, t_4/t = -0.1, t_5/t = -0.09, t_6/t = -0.2$  and the chemical potential  $\mu^*/t = 1.75$ .

Based on the above hopping parameters and Ref. [48], we used a value  $\alpha/t = 0.3$  for the strength of the ASOC. The Fermi surface of the two bands for this specific set of parameters is shown in Fig. 6.

#### A. Quasiparticles' contribution dominates in clean limit

The intensity of the THG signal in the clean limit is determined by

$$I_i^{\text{THG, clean}}(\omega) \propto |\chi_i^{\text{dia}}(\omega)|^2, \quad (64)$$

with the Coulomb-screened susceptibilities given in Eqs. (47)–(49), and shown in Fig. 7 for the quasiparticle ( $i = QP$ ), the Higgs ( $i = H$ ), and the Leggett response ( $i = \lambda$ ), respectively.



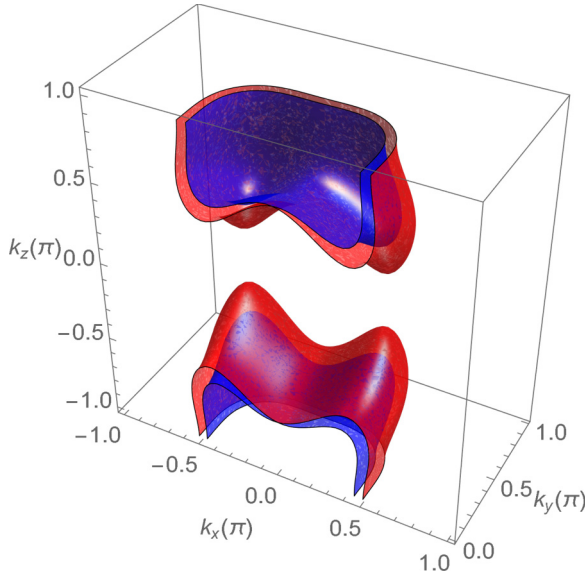


FIG. 6. Fermi surfaces of the noncentrosymmetric superconductor CePt<sub>3</sub>Si. 3D plot of the Fermi surfaces of the two bands ( $\mu = +1$  red,  $\mu = -1$  blue) of a noncentrosymmetric superconductor. For a better visibility only half of the total 3D Brillouin zone is shown here ( $0 < k_y < \pi$ ,  $-\pi < k_x, k_z < \pi$ ). The splitting of the two bands arises from the antisymmetric spin-orbit coupling term  $\mathbf{g}\mathbf{k}$ . The two bands are degenerate only along the  $z$  axis ( $k_x = k_y = 0$ ). The parameters used to obtain the Fermi surface are extracted from band structure calculations [48].

The THG signal contribution of the quasiparticle susceptibility is dominating the collective modes by several order of magnitudes for all shown triplet-singlet ratios  $p$ . The here investigated prototypical material CePt<sub>3</sub>Si shows a rather strong domination of the quasiparticles response compared to the Higgs response with a relative high THG intensity difference of  $I_{\text{QP}}/I_{\text{H}} \approx 10^6$ . It is important to note, that the exact relation between the quasiparticle response and the response of the collective modes is strongly related to the band structure around the Fermi level. In some other superconductors a stronger Higgs contribution was found; however, the general behavior of a dominating quasiparticle response in the clean limit was obtained so far in all investigated materials (see, e.g., Refs. [7,10]).

For  $p = 0.01$ , where the system can be approximated by an  $s$ -wave superconductor, the peak positions of the signal originated by different bands coincide, thus leading to a single peak structure at the THG resonance condition  $2\omega = 2\Delta_s$ . For increasing triplet-singlet ratio  $p$  the peak positions of both bands in the quasiparticle and Higgs response are drifting away from each other: for the  $\mu = +$  band the peak position can be well identified around  $2\omega = 2\Delta_+ = 2\Delta_s(1 + p)$ , while the peak position of band  $\mu = -$  is located at  $2\omega = 2\Delta_s(1 - p)$ . While at  $p = 0.25$  the second band becomes visible as a shoulder from the more prominent peak, the two-band structure can be seen especially well at  $p = 0.5$ . For that reason, we will use this specific triplet-singlet ratio later on for a more detailed analysis.

Physically more interesting is the region around  $p \approx 1$ , where the contribution of the singlet and triplet gap structure is

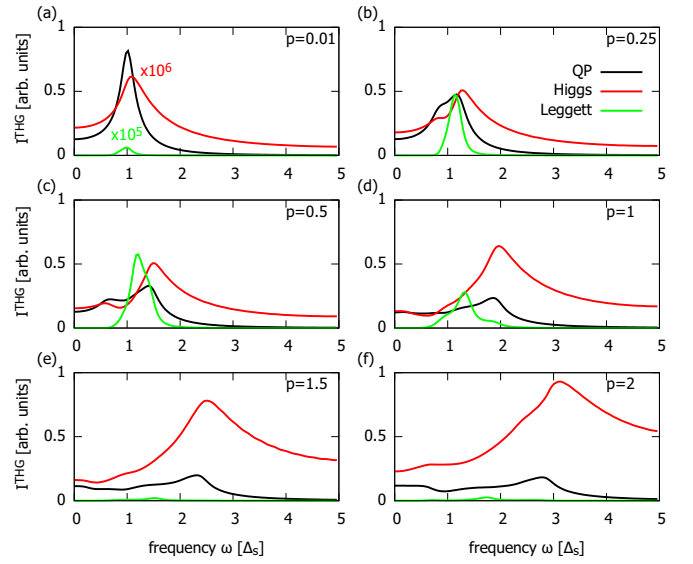


FIG. 7. Comparison of different THG signal contributions in the clean limit. THG signal contribution of the quasiparticles (black), Higgs mode (red,  $\times 10^6$ ), and Leggett mode (green,  $\times 10^5$ ) for different triplet-singlet ratios  $p$ . The single contributions are rescaled for a better comparison with the same factor in each panel. Note that the main contribution is always coming from the quasiparticles. With increasing triplet-singlet-parameter  $p$ , first a shoulder and then a two-peak structure is visible for the quasiparticles and the Higgs mode. The Leggett mode contributes only for small triplet-singlet-values ( $p < 1$ ) and vanishes when the triplet part dominates the gap structure.

on a similar level. In this regime we expect a balanced mixed parity gap in our system. In the proximity of  $p = 1$  most parts of the triplet and singlet gap are canceling with each other, so that we find the main contributions in the QP response of the  $\mu = -$  band around  $\omega \approx 0$ , resulting in a weak and very broad signal peaked at  $\omega = 0$ . As a result mainly the  $\mu = +$  band is seen in the response around  $2\omega = 2\Delta_+ = 4\Delta_s$ . Finally, in the triplet dominated regime (here, e.g., at  $p = 2$ ) the contribution of the band  $\mu = -$  is lifted up to  $2\omega = 2|\Delta_-| = 2\Delta_s(p - 1)$ . In this range it is very difficult to identify the lower energy band due to the fast changing gap value in the momentum space (see Fig. 2) resulting in rather strong broadening effects.

A more detailed frequency and temperature analysis of the quasiparticles is given in Fig. 8 for the THG intensity as well as the THG phase information. The typical BCS-like behavior of the two gaps  $\Delta_+$  and  $\Delta_-$  is clearly visible. Furthermore, a phase jump between the fundamental and the THG response can be detected at the resonance condition  $2\omega = 2\Delta_\mu$ . We will come back to the phase results later on, when comparing the phase signal under different circumstances in Sec. V A.

## B. Higgs modes

The qualitative analysis of the Higgs mode contribution follows the above described effects of the quasiparticle contribution, however at a quantitative significantly lower THG intensity. It is interesting to see, that with increasing triplet gap contributions the response of the Higgs mode increases compared to the quasiparticles. Nevertheless, also in

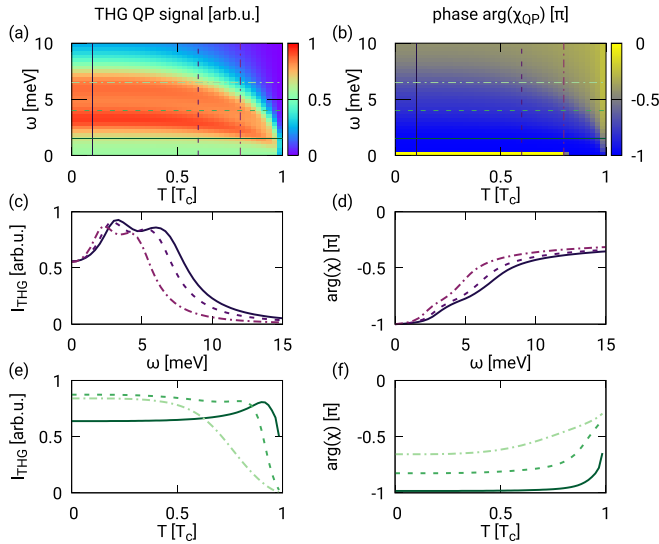


FIG. 8. Temperature dependence of THG intensity and phase: quasiparticles response. THG intensity (left column panels) and phase (right column panels) of the quasiparticle susceptibility for various frequencies and temperatures at the exemplary triplet-singlet ratio  $p = 0.5$ . (a) In the 2D plot the typical BCS-like behavior for the THG peak position is well visible. The two peak structure in the 2D plot becomes better visible, when looking at the constant temperature cuts in panel (c). These are taken at  $T = 0.1 T_c$  (solid),  $T = 0.6 T_c$  (dashed), and  $T = 0.8 T_c$  (dashed-pointed). For increasing temperature the peak position is shifted to lower frequencies. The constant frequency cuts in panel (e), which are experimentally easier to get are taken at  $\omega = 1.5$  meV (solid),  $\omega = 4$  meV (dashed) and  $\omega = 6.5$  meV (dashed-pointed). Unfortunately, the multippeak structure can not identified herein. (b) 2D diagram of the phase difference between the THG and the fundamental signal. At the peak position the phase is shifted by  $\approx +\pi/2$  (transition from blue to yellow). (d), (f) Constant temperature and frequency cuts of the phase differences at the same values used in panels (c), (e). In all cuts a phase jump at the resonance at  $\Delta\phi \approx \pi/2$  is well visible.

the limit of a triplet superconductor ( $p \rightarrow \infty$ ) the quasiparticle response is dominating by several orders of magnitudes.

As long as the system consists of a mixed parity gap structure, two Higgs modes (one for each band) can be clearly distinguished. Both modes are investigated in more detail in Figs. 9 and 10. We will first concentrate on Fig. 9, where the different contributions of the THG response of the Higgs signal are plotted individually. For the  $+$  and  $-$  band a peak can be seen in the spectrum (well visible, e.g., for  $p = 0.5$ ). The peak of the  $+$  band is still matching the corresponding frequency  $\omega = 2\Delta_+$ , while the peak in the  $-$  band can be identified at the corresponding frequency  $\omega = 2\Delta_-$ . The wide broadening of the peaks result not only from the strongly anisotropic gap behavior, but also from the coupling of the Higgs propagators  $H^{\mu\nu}$  ( $\mu \neq \nu$ ) of both bands, which leads to an admixture in their contributions. By analyzing the band-mixing contribution ( $\mu \neq \nu$ ) in this singlet-dominated regime in Fig. 9, it seems that we can not find an individual third peak in the spectrum. Instead the obtained features in the THG susceptibility are only appearing from adding the weighted contributions from the  $+$  and  $-$  band susceptibilities.

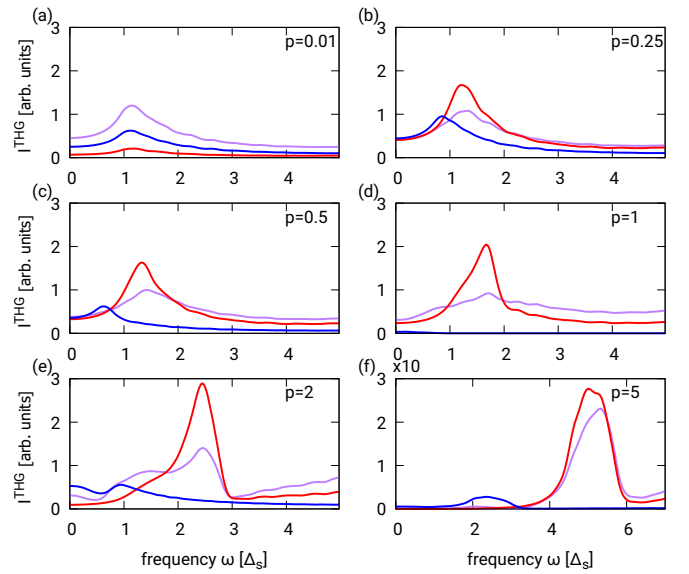


FIG. 9. THG signal of the Higgs contribution in the clean limit. THG signal contribution of the Higgs mode for various triplet-singlet ratios  $p$ : the contribution from the band  $\mu = +1$  is shown in red,  $\mu = -1$  in blue and the band-mixing contribution in purple. (a)–(d) For increasing values of the triplet-singlet-ratio  $p$ , the  $\mu = +1$  band contribution is dominant with respect to both the  $\mu = -1$  band and the band mixing contribution. While the peak position of the Higgs mode in the  $\mu = -1$  band is shifting to lower frequencies from the  $s$ -band resonance condition  $2\omega < 2\Delta_s$ , the new resonance condition for the  $\mu = +1$  band is above the original frequency  $2\omega > 2\Delta_s$ . (e), (f) In the limit of high triplet contribution to the gap ( $p \gg 1$ ), the Higgs mode in the  $\mu = -1$  band is almost suppressed by the  $\mu = +1$  band mode.

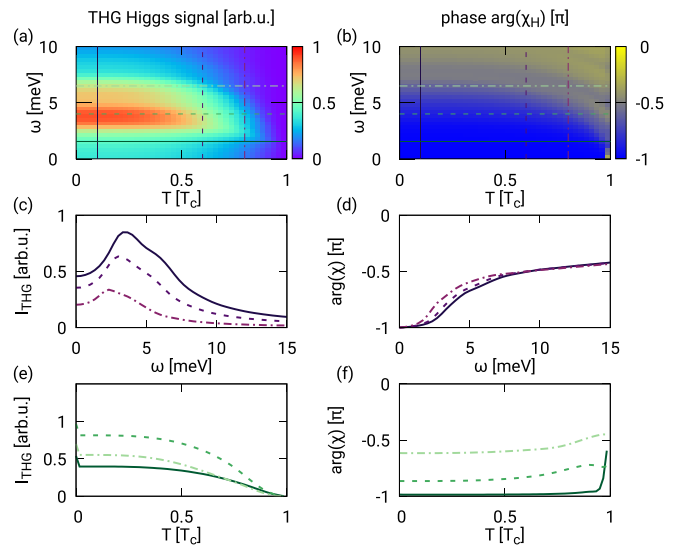


FIG. 10. Temperature dependence of THG intensity and phase: Higgs mode. THG intensity (left column panels) and phase (right column panels) of the Higgs mode contribution for various frequencies and temperatures at the exemplary triplet-singlet ratio  $p = 0.5$ . The temperature and frequency cuts [solid and dashed lines in (c)–(f)] are taken at the exact same values as introduced for the quasiparticles in Fig. 8. The qualitative results match those of the quasiparticles contribution calculations.

While in the singlet gap structure dominated regime ( $p < 1$ ) the spectra shows exactly one mode at each band, the situation becomes more interesting, when increasing the triplet-singlet ratio ( $p > 1$ ). At  $p = 2$ , one can find next to the single peak structure of the  $\mu = +$  band, a multiple peak structure in the  $\mu = -$  band. The multiple peak structure can be explained with the help of the gap symmetry in Fig. 2. For small triplet-singlet ratios  $p < 1$ , there are no nodes appearing in the gap structure of the  $\mu = -$  band. Increasing the triplet-singlet ratio over the critical value of  $p = 1$ , leads to the appearance of nodes and hence lobes of similar size in the different  $\mathbf{k}$ -directions [see exemplary Fig. 2(e) at  $p = 2$ ]. This results in equal contributions of the lobes to the total gap function. This competition is in the end responsible for the occurring of multiple peaks in the THG response. A similar behavior is for example also visible for the  $d$ -wave gap symmetry in [12]. In the limit of a triplet superconductor  $p \gg 1$ , we obtain again only a single peak structure in the  $\mu = -$  band. Additionally, in this limit the  $\mu = -$  band contributions are overshadowed by the  $\mu = +$  band response, due to the large difference of the average gap value.

Analyzing the 2D-frequency-temperature results in Fig. 10 the THG response still reproduces the typical BCS-gap behavior. However, in contrast to the quasiparticle response, we find a strong decrease of the Higgs mode intensity for increasing temperatures  $T$ . This leads to an even stronger domination of the quasiparticles close to the critical temperature  $T_c$ .

### C. Leggett mode

Additional to the two Higgs modes, the effective two-band structure in noncentrosymmetric superconductors enable the appearance of an additional third mode, namely the Leggett mode in the system. This mode corresponds to the relative phase oscillations between the two bands and is not effected by the Anderson-Higgs mechanism or the sum-phase oscillations. The existence of the Leggett mode in noncentrosymmetric superconductors was already proposed by Ref. [19], where the dispersion was derived. Dependent on the inter- ( $V_{+-}$ ) and intraband ( $V_{++}, V_{--}$ ) interaction strength of the two bands the Leggett mode exists either below the two Higgs modes ( $V_{\mu\mu} \gg V_{+-}$ ) or in between the two Higgs modes for sufficient strong interband couplings  $V_{+-}$ . For the prototypical noncentrosymmetric superconductor, which we have analyzed, the interaction strength is large enough to find a well pronounced Leggett mode in between the two Higgs modes.

In the limit of small triplet-singlet ratios  $p$  the Leggett mode is visible slightly above the  $s$ -wave gap energy  $2\omega \geq 2\Delta_s$ . In this singlet dominated regime the THG intensity of the Leggett mode is clearly higher compared to the Higgs mode ( $I_\lambda/I_H \approx 10^2$ ). However, in the limit of strong triplet contributions the Leggett mode vanishes. This behavior can be justified, by the strong unequal contributions of the two different bands in this regime, which was already visible for the QP and Higgs response.

In Fig. 11 the single resonance structure in the THG intensity is visible in a 2D plot over temperature and frequency. Due to the single-peak structure of the spectrum, the Leggett mode is noticeably pronounced compared to the correspond-

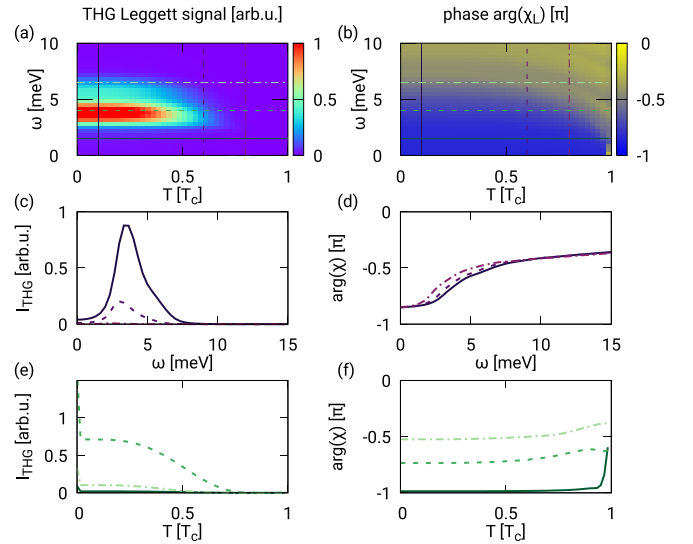


FIG. 11. Temperature dependence of THG intensity and phase: Leggett mode. THG intensity (left column panels) and phase (right column panels) of the Leggett mode contribution for various frequencies and temperatures at the exemplary triplet-singlet ratio  $p = 0.5$ . The temperature and frequency cuts [solid and dashed lines in (c)–(f)] are taken at the exact same values as introduced for the quasiparticles and Higgs contribution calculations. However, instead of a multipeak behavior, we can identify the single Leggett mode by a sharp peak.

ing QP and Higgs response. Similar to the Higgs THG signal we find a strong decrease of the intensity by increasing temperature  $T$ . Close to the critical temperature  $T_c$  the Leggett mode vanishes.

## V. RESULTS IN THE DIRTY LIMIT: ENHANCEMENT OF HIGGS MODES

So far, only the THG response in the clean limit was analyzed. When including impurities to our system additional contributions from the paramagnetic response appear in the THG signal. This paramagnetic response which vanishes in the clean limit dominates the diamagnetic response already when including only a small amount of impurities. As a result we can find a strong enhancement of the collective modes compared to the quasiparticle response. For dirty noncentrosymmetric superconductors, we can find therefore Higgs modes almost at the same magnitude as the quasiparticle, so that the Higgs modes should also be experimentally well detectable in these systems.

The THG response in the dirty limit is calculated by

$$I_i^{\text{THG, dirty}}(\omega) \propto |\chi_i^{\text{para}}(\omega)|^2, \quad (65)$$

with the Coulomb-screened susceptibilities given in Eqs. (56)–(58) for the quasiparticle ( $i = \text{QP}$ ), the Higgs ( $i = \text{H}$ ) and the Leggett response ( $i = \lambda$ ), respectively. In Fig. 12, we are comparing the signal strength of the different contributions in the clean and dirty limit for various triplet-singlet ratios  $p$ .

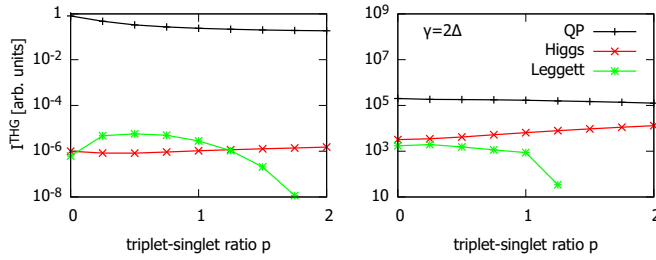


FIG. 12. Comparison of peak positions in clean and dirty superconductors. The THG intensity of the peaks of the quasiparticle (black), Higgs mode (red) and Leggett mode (green) are compared in clean and dirty ( $\gamma = 2\Delta$ ) superconductors. (a) In the diamagnetic coupling (the only coupling allowed in clean superconductors) the quasiparticle response dominates the collective modes by various orders of magnitudes ( $I_{QP}/I_H \approx 10^6$ ) for all triplet-singlet values  $p$ . Here the vanishing of the Leggett mode in the triplet regime  $p > 1.5$  is well visible. (b) In the paramagnetic coupling (the main source for dirty superconductors) the intensity coming from the Higgs modes converges to the quasiparticle response intensity, especially for high triplet-singlet ratios  $p > 1$  ( $I_{QP}/I_H \approx 10^1-10^2$ ). The Leggett mode is vanishing even faster in this configuration. For a better comparison we use the normalization of  $I_{QP}^{THG}(p=0, \gamma=0) = 1$  and adjust the other THG intensities accordingly.

As already mentioned a strong enhancement of the collective modes compared to the clean limit is visible for all triplet-singlet values  $p$ . This behavior was already obtained in centrosymmetric superconductors [42–44]. Our results may be seen as a generalization of their results to NCS. Furthermore, it is remarkable that in the dirty limit the resonance intensity of the Higgs mode and the resonance intensity in the quasiparticle response are approaching each other for increasing triplet-singlet ratio  $p$ . Unfortunately, we could not find an exceeding Higgs intensity in the investigated regime. However, the Leggett mode is vanishing already for smaller triplet contributions ( $p \approx 1$ ) compared to the clean limit.

Note, that only a small impurity strength  $\gamma$  is enough, so that the paramagnetic response is dominating the diamagnetic response and therefore a strong enhancement of the collective modes is present. This behavior is visible also in Fig. 13 where the intensity of the contributions is plotted over the impurity strength  $\gamma$ . With increasing impurity strength, one obtains a similar trend of an approaching Higgs mode intensity to the quasiparticle contributions. In contrast, the intensity of the Leggett mode is peaked around  $\gamma \approx 2\Delta^+$  and vanishes much faster in the dirty limit, as it is highly affected by the interband interaction. As a result we can summarize that the Higgs mode is best visible in the dominating triplet regime with a strong influence of the impurities.

### A. Phase signal for THG

Next to the THG intensity, also the phase difference between the fundamental response and the THG response show meaningful information. In previous works, it was already possible to indicate a coupling between collective modes via an antiresonance behavior of this phase difference experimentally [41]. Additionally, for trivial even parity gap

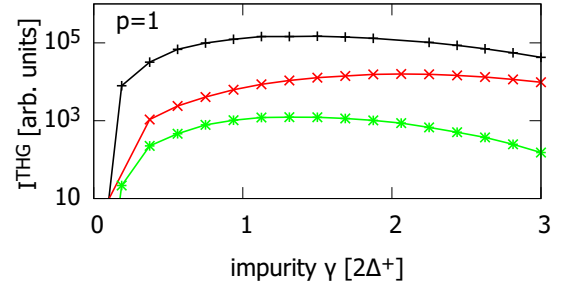


FIG. 13. Impurity dependence of THG intensity. THG intensity for different orders of impurities  $\gamma$  for a balanced ratio between singlets and triplets  $p = 1$ . Only a small amount of impurities leads to a strong enhancement of the overall signal and additionally to an enhancement of the collective mode contributions compared to the quasiparticles (black). While the Leggett mode decreases (green) in the strong dirty limit, the Higgs mode (red) contributions can compete with the quasiparticle response in this limit. The same normalization as in Fig. 12 is used.

structures at the resonance condition  $2\omega = 2\Delta$  of a collective mode a phase jump was already calculated in the spectra, which exhibits a sudden rise, when including impurities to the system [11,47].

To identify the above-mentioned phenomena in the phase information, we calculate the phase of the THG response in relation to the response of the first harmonic generation. The THG phase jump at the Higgs mode resonance in the clean limit is shown in the 2D plot in Fig. 10 for various frequencies and temperatures at the exemplary triplet-singlet ratio  $p = 0.5$ . At the resonance condition the phase is shifted by  $\sim +\pi/2$ . This value can be understood by analyzing the Higgs propagator which can be approximated at least close to the  $p = 0$  limit to a form of

$$H(\omega) \propto \frac{1}{\sqrt{4\Delta^2 - \omega^2}}. \quad (66)$$

This resonance condition is in contrast to classical oscillators, where the resonance occurs due to a  $1/(\omega_0^2 - \Omega^2)$  factor and leading to a  $\pi$ -phase jump at the resonance. The square root in the Higgs propagator reduces therefore the phase jump at the resonance by a factor of 2. Note that a similar behavior can be seen for the other visible THG resonances in the clean limit for quasiparticles in Fig. 8 and for the Leggett mode in Fig. 11.

When including impurities, as expected, a sudden rise of the phase jump in the THG signal occurs at the peak positions [47] (see Fig. 14). At the resonance we can find in these cases an increased phase jump of  $\sim \pi$  due to the inclusion of the paramagnetic diagrams in the system. This leads to an additional contribution from the electron-mediated microscopic coupling of light to the Higgs mode, which effects the resulting phase jump. This phenomena, which is already visible for small amounts of impurities can be used to distinguish Higgs modes in the system even if they are suppressed by orders of magnitudes.



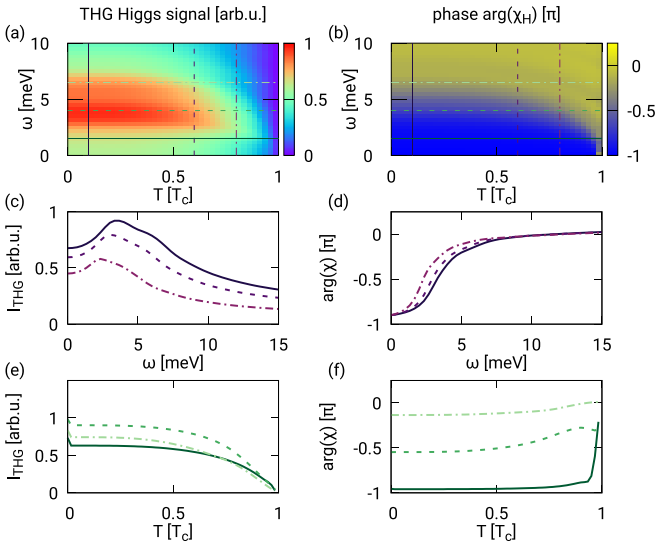


FIG. 14. Temperature dependence of THG intensity and phase: Higgs mode in dirty limit. THG intensity (left column panels) and phase (right column panels) of the Higgs mode contribution for various frequencies and temperatures at the exemplary triplet-singlet ratio  $p = 0.5$  in the dirty limit. (a) Similar to the clean limit in Fig. 10 the 2D plot the typical BCS-like behavior for the THG peak position is well visible. (c) Constant temperature cuts are taken at  $T = 0.1 T_c$  (solid),  $T = 0.6 T_c$  (dashed) and  $T = 0.8 T_c$  (dashed-pointed) to increase the visibility of the two-peak structure. The constant frequency cuts in (e) are taken at  $\omega = 1.5$  meV (solid),  $\omega = 4$  meV (dashed) and  $\omega = 6.5$  meV (dashed-pointed). (b) 2D diagram of the phase difference between the THG and the fundamental signal. The major difference to the clean limit case is that the phase is shifted here by  $\pi$  instead of  $\pi/2$ . (d), (f) This behavior gets better visible when looking at the constant temperature and frequency cuts of the phase differences at the same values used in panels (c), (e). In all cuts a phase jump at the resonance at  $\Delta\phi \approx \pi$  is well visible.

## VI. COMPARISON WITH PREVIOUS WORK

A detailed analysis of the THG intensity and phase were already found in the paper by Schwarz *et al.* [47]. However, this analysis covered only the  $s$ - and  $d$ -wave gap symmetry. Our studies in this work go beyond the simple case of spin-singlet superconductors. Due to the missing center of inversion, a superposition of singlet and triplet components occurs. This yields a more complicated THG response than in previous studies. However, we can see that similar to the previous work the quasiparticle response dominates the Higgs mode for clean superconductors, while for dirty superconductors the Higgs mode get enhanced. The exact factor of the enhancement is difficult to compare, since the band structure plays an important role herein. In contrast to the  $s$ -wave case, we find now two distinct Higgs modes at frequencies corresponding to the two emerged bands in noncentrosymmetric superconductors. The resonance conditions for these Higgs modes of the both bands  $\mu$  are related to their actual gap value  $2\omega_\mu = 2\Delta_\mu$  with  $\Delta_\mu = \sum_{\mathbf{k}} |\Delta_\mu(\mathbf{k})|$ , respectively.

Importantly, due to the multiband structure of our system, a Leggett mode is appearing in the THG response. An occurrence of such a relative phase mode in the THG response was already discussed in references [1,11]. However, in these

works the Leggett mode (especially in the dirty superconducting case) was controlled by the interband coupling of an even-parity multiband superconductor, such as  $\text{MgB}_2$ . On the contrary, in NCS the Kramers spin degeneracy is lifted due to the presence of the asymmetric spin-orbit coupling. As a result the two bands are no longer described in the originally spin basis. Consequently, the interband coupling is closely related to the triplet-singlet ratio  $p$  in the system. Thus we find, that in contrast to the Higgs mode, the strength of the Leggett mode is strongly sensitive on the detailed spin properties material, which was is not the case in a spin-singlet multiband superconductor.

Furthermore, we want to emphasize that the determined values of the phase jump of the Higgs mode in clean and dirty superconductors from previous works [7,47] are also confirmed for NCS systems. As a result, it is possible to use phase measurements of the THG signal to proof the presence of Higgs modes. From these kind of measurements one can gain useful information about the modes even if the amplitude of the corresponding modes is highly suppressed by other phenomena (e.g., phonons) at the same energy. Although, the general presence of a Higgs mode can be identified, the resulting interplay between modes from different bands in the phase signal, such as antiresonances (see, e.g., Ref. [41]) are hard to identify in NCS. The reason for that is the strong overlap of the gap structure in the two bands, thus their respective contributions can not be distinguished in these kind of compounds, as it was possible, e.g., in Ref. [47]. For detailed investigations in this direction we refer to systems, where Higgs modes couple to additional external modes with a different origin such as CDW. Even in the limit of a strong triplet contribution  $p \gg 1$  phenomena of that kind will be suppressed, due to a strongly dominant  $\mu = +$  band Higgs response in that regime.

Finally, we comment on the recently found collective modes for NCS in the second harmonic generation (SHG) signal [40]. In the here chosen formalism, it is not possible to find a Higgs response in SHG. The reason for that is the unitary choice of a parallel ASOC and the triplet gap function  $\mathbf{g}_{\mathbf{k}} \parallel \mathbf{d}_{\mathbf{k}}$  as presented in Refs. [17,20,21]. Only, when violating this unitary condition, one can obtain a nonvanishing contribution in the SHG from Higgs modes. So far, as one could assume, observations have shown a strong suppression of this specific triplet gap contribution in NCS. So we conclude, that THG is the lowest order signal that can be measured in NCS systems.

## VII. CONCLUSION

In this paper we have extended the study of the collective modes, here namely the Higgs mode and the Leggett mode, to a new class of materials, the noncentrosymmetric superconductors. In doing so, we calculated the response of the third harmonic generation via an effective action approach and a diagrammatic approach in the clean limit as well as in the influence of impurities.

We have shown that next to the usual quasiparticle response in THG collective modes contribute to the spectra. The hereby studied collective modes consist of three distinguishable modes, namely two Higgs modes at  $2\omega_1 = 2\Delta_+$  and  $2\omega_2 = 2\Delta_-$ , respectively, and a relative phase mode



(or Leggett mode) around the  $s$ -wave gap value  $2\omega = 2\Delta_s$ . While in the clean limit the response of the collective modes is comparable small, their response enhance dramatically when including only a small amount of impurities. Note, that the Leggett mode will appear only for small triplet-singlet ratios or in other words only if the coupling between the two bands is strong enough.

As in previous studies [1,11,41,47] the phase difference between incoming and THG signal is an important parameter to reflect the cleanness of the superconductor. While a phase jump at the resonance of  $\pi/2$  can be found in the clean limit, the phase jump rises to  $\pi$  when including paramagnetic contributions as observed in the dirty limit.

Our THG results clearly demonstrate that noncentrosymmetric superconductors can be used as an important material class to get more insights, theoretically as well as experimentally about the Higgs mode and other collective modes such as the Leggett mode. In particular, the Leggett mode reacts very sensitive to the so far unknown triplet-singlet ratio of the most NCS materials. Another interesting point is the strength of impurities, which can be used to optimize the system to a strong Higgs contribution compared to the quasiparticles. We remark that in our analysis the THG signal, is the lowest excitation order in the system, as the SHG signal vanishes under the rational condition  $\mathbf{g}_\mathbf{k} \parallel \mathbf{d}_\mathbf{k}$ .

We are aware that in practice the optical experiments with NCS materials are difficult to perform, due to the small critical temperature  $T_c$  in combination with the unavoidable heating of the sample. Especially, the usage of the prototypical compound CePt<sub>3</sub>Si is a challenge as it has a comparable small  $T_c \approx 1.7$  K. Fortunately, qualitatively similar results are expected not only for compounds with the same crystal symmetry, but also for other point groups with higher  $T_c \approx 10$  K, such as Li<sub>2</sub>Pd<sub>x</sub>Pt<sub>3-x</sub>B or Re<sub>3</sub>W. Here, we point the focus to the exemplary material of Li<sub>2</sub>Pt<sub>3</sub>B, where the existence of a dominating triplet gap is already known.

#### ACKNOWLEDGMENTS

Special thanks to Matteo Puviani, who helped formulating the problem. Fruitful discussions with Lukas Schwarz,

Rafael Haenel, Sida Tian, Silvia Neri, and Jakob Dolgner are thankfully acknowledged. We also thank Elio König for critical reading of the manuscript. We thank the Max Planck-UBC-UTokyo Center for Quantum Materials for financial support.

#### APPENDIX: NOTATION AND NAMBU GREEN'S FUNCTIONS

In our description we make use of the Nambu-Gor'kov spinor  $\Psi_{\mathbf{k},\mu}^\dagger = (\hat{c}_{\mathbf{k},\mu}^\dagger \hat{c}_{-\mathbf{k},\mu})$ , so that we can write the full Hamiltonian as

$$\hat{H} = \frac{1}{2} \sum_{\mathbf{k}} \sum_{\mu=\pm 1} \xi_{\mathbf{k},\mu} \Psi_{\mathbf{k},\mu}^\dagger \tau_3 \Psi_{\mathbf{k},\mu} + \frac{1}{4} \sum_{\mathbf{k},\mathbf{k}'} \sum_{\mu,\nu=\pm 1} V_{\mu,\nu;\mathbf{k},\mathbf{k}'} \times \Psi_{\mathbf{k},\mu}^\dagger (\tau_1 + i\tau_2) \Psi_{\mathbf{k},\mu} \Psi_{\mathbf{k}',\nu}^\dagger (\tau_1 - i\tau_2) \Psi_{\mathbf{k}',\nu}, \quad (\text{A1})$$

with the Pauli matrices

$$\tau_1 = \begin{pmatrix} 0 & 1 \\ 1 & 0 \end{pmatrix}, \quad \tau_2 = \begin{pmatrix} 0 & -i \\ i & 0 \end{pmatrix}, \quad \tau_3 = \begin{pmatrix} 1 & 0 \\ 0 & -1 \end{pmatrix}.$$

Therefore, the 2-fermions interaction terms can be written with electron creation and annihilation operators as follows:

$$\Psi_{\mathbf{k},\mu}^\dagger (\tau_1 + i\tau_2) \Psi_{\mathbf{k},\mu} = \hat{c}_{\mathbf{k},\mu}^\dagger \hat{c}_{-\mathbf{k},\mu}^\dagger, \quad (\text{A2a})$$

$$\Psi_{\mathbf{k}',\nu}^\dagger (\tau_1 - i\tau_2) \Psi_{\mathbf{k}',\nu} = \hat{c}_{-\mathbf{k},\nu} \hat{c}_{\mathbf{k},\nu}. \quad (\text{A2b})$$

The Green's function of the superconducting state in Nambu-Gor'kov space can be written in the matricial form

$$G_\mu(\mathbf{k}, iv_m) = \frac{1}{(iv_m)^2 - E_{\mathbf{k},\mu}^2} \cdot \begin{pmatrix} iv_m + \xi_{\mathbf{k},\mu} & \Delta_{\mathbf{k},\mu} \\ \Delta_{\mathbf{k},\mu}^* & iv_m - \xi_{\mathbf{k},\mu} \end{pmatrix}, \quad (\text{A3})$$

or, using the Pauli matrices,

$$G_\mu(\mathbf{k}, iv_m) = \frac{iv_m \tau_0 + \xi_{\mathbf{k},\mu} \tau_3 + (\Delta'_{\mathbf{k},\mu} \tau_1 - \Delta''_{\mathbf{k},\mu} \tau_2)}{(iv_m)^2 - E_{\mathbf{k},\mu}^2}, \quad (\text{A4})$$

with the complex order parameter  $\Delta_{\mathbf{k},\mu} = \Delta'_{\mathbf{k},\mu} + i\Delta''_{\mathbf{k},\mu}$ .

- 
- [1] N. Tsuji and H. Aoki, Theory of Anderson pseudospin resonance with Higgs mode in superconductors, *Phys. Rev. B* **92**, 064508 (2015).
- [2] N. Tsuji and Y. Nomura, Higgs-mode resonance in third harmonic generation in NBN superconductors: Multiband electron-phonon coupling, impurity scattering, and polarization-angle dependence, *Phys. Rev. Res.* **2**, 043029 (2020).
- [3] T. Cea and L. Benfatto, Nature and Raman signatures of the Higgs amplitude mode in the coexisting superconducting and charge-density-wave state, *Phys. Rev. B* **90**, 224515 (2014).
- [4] T. Cea, C. Castellani, and L. Benfatto, Nonlinear optical effects and third-harmonic generation in superconductors: Cooper pairs versus Higgs mode contribution, *Phys. Rev. B* **93**, 180507(R) (2016).
- [5] M. Udina, T. Cea, and L. Benfatto, Theory of coherent-oscillations generation in terahertz pump-probe spectroscopy: From phonons to electronic collective modes, *Phys. Rev. B* **100**, 165131 (2019).
- [6] J. Fiore, M. Udina, M. Marciani, G. Seibold, and L. Benfatto, Contribution of collective excitations to third harmonic generation in two-band superconductors: The case of MgB<sub>2</sub>, *Phys. Rev. B* **106**, 094515 (2022).
- [7] L. Schwarz and D. Manske, Theory of driven Higgs oscillations and third-harmonic generation in unconventional superconductors, *Phys. Rev. B* **101**, 184519 (2020).
- [8] M. Puviani, L. Schwarz, X.-X. Zhang, S. Kaiser, and D. Manske, Current-assisted Raman activation of the Higgs mode in superconductors, *Phys. Rev. B* **101**, 220507(R) (2020).

- [9] M. Puviani, A. Baum, S. Ono, Y. Ando, R. Hackl, and D. Manske, Calculation of an enhanced  $A_{1g}$  symmetry mode induced by Higgs oscillations in the Raman spectrum of high-temperature cuprate superconductors, *Phys. Rev. Lett.* **127**, 197001 (2021).
- [10] Y. Murotani and R. Shimano, Nonlinear optical response of collective modes in multiband superconductors assisted by non-magnetic impurities, *Phys. Rev. B* **99**, 224510 (2019).
- [11] R. Haenel, P. Froese, D. Manske, and L. Schwarz, Time-resolved optical conductivity and Higgs oscillations in two-band dirty superconductors, *Phys. Rev. B* **104**, 134504 (2021).
- [12] L. Schwarz, B. Fauseweh, N. Tsuji, N. Cheng, N. Bittner, H. Krull, M. Berciu, G. S. Uhrig, A. P. Schnyder, S. Kaiser, and D. Manske, Classification and characterization of nonequilibrium Higgs modes in unconventional superconductors, *Nat. Commun.* **11**, 287 (2020).
- [13] Y. Murotani, N. Tsuji, and H. Aoki, Theory of light-induced resonances with collective Higgs and Leggett modes in multiband superconductors, *Phys. Rev. B* **95**, 104503 (2017).
- [14] N. R. Poniatowski, J. B. Curtis, A. Yacoby, and P. Narang, Spectroscopic signatures of time-reversal symmetry breaking superconductivity, *Commun Phys* **5**, 44 (2022).
- [15] V. P. Mineev and K. V. Samokhin, *Unconventional Superconductivity* (Gordon and Breach Science Publishers, London, UK, 1999).
- [16] L. P. Gor'kov and E. I. Rashba, Superconducting 2D system with lifted spin degeneracy: Mixed singlet-triplet state, *Phys. Rev. Lett.* **87**, 037004 (2001).
- [17] P. Frigeri, D. Agterberg, and I. E. Milat, Phenomenological theory of the  $s$ -wave state in superconductors without an inversion center, *Eur. Phys. J. B* **54**, 435 (2006).
- [18] E. Bauer and M. Sigrist, *Non-centrosymmetric Superconductors* (Springer-Verlag, Berlin, 2012).
- [19] N. Bittner, D. Einzel, L. Klam, and D. Manske, Leggett modes and the Anderson-Higgs mechanism in superconductors without inversion symmetry, *Phys. Rev. Lett.* **115**, 227002 (2015).
- [20] P. A. Frigeri, D. F. Agterberg, A. Koga, and M. Sigrist, Superconductivity without inversion symmetry: MnSi versus CePt<sub>3</sub>Si, *Phys. Rev. Lett.* **92**, 097001 (2004).
- [21] P. A. Frigeri, D. F. Agterberg, and M. Sigrist, Spin susceptibility in superconductors without inversion symmetry, *New J. Phys.* **6**, 115 (2004).
- [22] K. V. Samokhin, Magnetic properties of superconductors with strong spin-orbit coupling, *Phys. Rev. B* **70**, 104521 (2004).
- [23] K. V. Samokhin, E. S. Zijlstra, and S. K. Bose, CePt<sub>3</sub>Si: An unconventional superconductor without inversion center, *Phys. Rev. B* **69**, 094514 (2004).
- [24] K. V. Samokhin, Paramagnetic properties of noncentrosymmetric superconductors: Application to CePt<sub>3</sub>Si, *Phys. Rev. Lett.* **94**, 027004 (2005).
- [25] K. V. Samokhin and V. P. Mineev, Gap structure in noncentrosymmetric superconductors, *Phys. Rev. B* **77**, 104520 (2008).
- [26] V. P. Mineev and K. V. Samokhin, Nonuniform states in noncentrosymmetric superconductors: Derivation of Lifshitz invariants from microscopic theory, *Phys. Rev. B* **78**, 144503 (2008).
- [27] P. Thalmeier, A. Akbari, Full  $t$ -matrix approach to quasiparticle interference in non-centrosymmetric superconductors, *Eur. Phys. J. B* **86**, 495 (2013).
- [28] P. Thalmeier and A. Akbari, Rashba spin-orbit coupling effects in quasiparticle interference of non-centrosymmetric superconductors, *Europhys. Lett.* **102**, 57008 (2013).
- [29] E. Bauer, G. Hilscher, H. Michor, C. Paul, E. W. Scheidt, A. Gribanov, Y. Seropegin, H. Noël, M. Sigrist, and P. Rogl, Heavy fermion superconductivity and magnetic order in non-centrosymmetric CePt<sub>3</sub>Si, *Phys. Rev. Lett.* **92**, 027003 (2004).
- [30] C. F. Miclea, A. C. Mota, M. Nicklas, R. Cardoso, F. Steglich, M. Sigrist, A. Prokofiev, and E. Bauer, Extreme vortex pinning in the noncentrosymmetric superconductor CePt<sub>3</sub>Si, *Phys. Rev. B* **81**, 014527 (2010).
- [31] J. S. Kim, D. J. Mixson, D. J. Burnette, T. Jones, P. Kumar, B. Andraka, G. R. Stewart, V. Craciun, W. Acree, H. Q. Yuan, D. Vandervelde, and M. B. Salamon, Spurious second transition in the heavy-fermion superconductor CePt<sub>3</sub>Si, *Phys. Rev. B* **71**, 212505 (2005).
- [32] A. Amato, E. Bauer, and C. Baines, Coexistence of magnetism and superconductivity in the heavy-fermion superconductor CePt<sub>3</sub>Si, *Phys. Rev. B* **71**, 092501 (2005).
- [33] G. M. Luke, A. Keren, K. Kojima, L. P. Le, B. J. Sternlieb, W. D. Wu, Y. J. Uemura, Y. Ōnuki, and T. Komatsubara, Competition between magnetic order and superconductivity in CeCu<sub>2.2</sub>Si<sub>2</sub>, *Phys. Rev. Lett.* **73**, 1853 (1994).
- [34] M. Nicklas, F. Steglich, J. Knolle, I. Eremin, R. Lackner, and E. Bauer, Pair breaking by nonmagnetic impurities in the noncentrosymmetric superconductor CePt<sub>3</sub>Si, *Phys. Rev. B* **81**, 180511(R) (2010).
- [35] K. Izawa, Y. Kasahara, Y. Matsuda, K. Behnia, T. Yasuda, R. Settai, and Y. Onuki, Line nodes in the superconducting gap function of noncentrosymmetric CePt<sub>3</sub>Si, *Phys. Rev. Lett.* **94**, 197002 (2005).
- [36] M. Yogi, Y. Kitaoka, S. Hashimoto, T. Yasuda, R. Settai, T. D. Matsuda, Y. Haga, Y. Ōnuki, P. Rogl, and E. Bauer, Evidence for a novel state of superconductivity in noncentrosymmetric CePt<sub>3</sub>Si: A <sup>195</sup>Pt-NMR study, *Phys. Rev. Lett.* **93**, 027003 (2004).
- [37] M. Smidman, M. B. Salamon, H. Q. Yuan, and D. F. Agterberg, Superconductivity and spin-orbit coupling in non-centrosymmetric materials: A review, *Rep. Prog. Phys.* **80**, 036501 (2017).
- [38] T. Cea and L. Benfatto, Signature of the Leggett mode in the  $A_{1g}$  Raman response: From MgB<sub>2</sub> to iron-based superconductors, *Phys. Rev. B* **94**, 064512 (2016).
- [39] L. Klam, D. Einzel, and D. Manske, Electronic Raman scattering in noncentrosymmetric superconductors, *Phys. Rev. Lett.* **102**, 027004 (2009).
- [40] H. Tanaka, H. Watanabe, and Y. Yanase, Nonlinear optical responses in noncentrosymmetric superconductors, *Phys. Rev. B* **107**, 024513 (2023).
- [41] H. Chu, M.-J. Kim, K. Katsumi, S. Kovalev, R. D. Dawson, L. Schwarz, N. Yoshikawa, G. Kim, D. Putzky, Z. Z. Li, H. Raffy, S. Germanskiy, J.-C. Deinert, N. Awari, I. Ilyakov, B. Green, M. Chen, M. Bawatna, G. Cristiani, G. Logvenov *et al.*, Phase-resolved Higgs response in superconducting cuprates, *Nat. Commun.* **11**, 1793 (2020).
- [42] M. Silaev, Nonlinear electromagnetic response and Higgs-mode excitation in BCS superconductors with impurities, *Phys. Rev. B* **99**, 224511 (2019).

- [43] G. Seibold, M. Udina, C. Castellani, and L. Benfatto, Third harmonic generation from collective modes in disordered superconductors, *Phys. Rev. B* **103**, 014512 (2021).
- [44] K. Katsumi, J. Fiore, M. Udina, R. R. I. au2, D. Barbalas, J. Jesudasan, P. Raychaudhuri, G. Seibold, L. Benfatto, and N. P. Armitage, Revealing novel aspects of light-matter coupling in terahertz two-dimensional coherent spectroscopy: The case of the amplitude mode in superconductors, *Phys. Rev. Lett.* **132**, 256903 (2024).
- [45] E. Rashba, Properties of semiconductors with an extremum loop. I. Cyclotron and combinational resonance in a magnetic field perpendicular to the plane of the loop, *Sov. Phys.-Solid State* **2**, 1109 (1960).
- [46] D. C. Mattis and J. Bardeen, Theory of the anomalous skin effect in normal and superconducting metals, *Phys. Rev.* **111**, 412 (1958).
- [47] L. Schwarz, R. Haenel, and D. Manske, Phase signatures in the third-harmonic response of Higgs and coexisting modes in superconductors, *Phys. Rev. B* **104**, 174508 (2021).
- [48] Y. Yanase and M. Sigrist, Non-centrosymmetric superconductivity and antiferromagnetic order: Microscopic discussion of CePt3Si, *J. Phys. Soc. Jpn.* **76**, 043712 (2007).